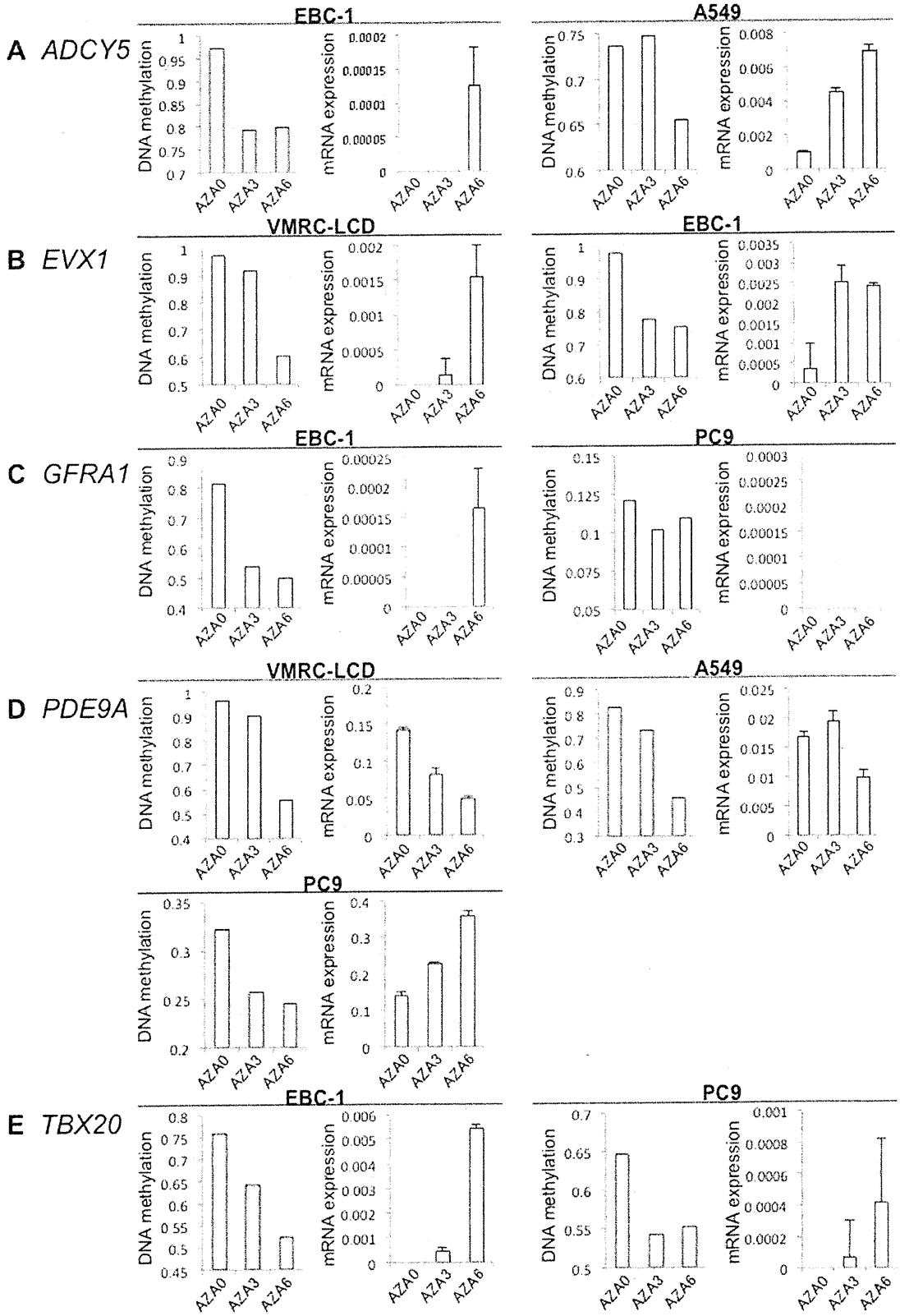
A ADCY5
EBC-1
A549
B EVX1
VMRC-LCD
EBC-1
C GFRA1
EBC-1
PC9
D PDE9A
VMRC-LCD
A549
PC9
E TBX20
EBC-1
PC9
DNA methylation
mRNA expression
AZA0
AZA3
AZA6

**Figure 3. DNA methylation levels and mRNA expression levels after 5-aza-2′-deoxycytidine (5-aza-dC) treatment.** DNA methylation levels (β-values) and mRNA expression levels for the *ADCY5* (**A**), *EVX1* (**B**), *GFRA1* (**C**), *PDE9A* (**D**) and *TBX20* (**E**) genes were determined by Infinium assay and quantitative real-time reverse transcription-PCR analysis, respectively. The error bars represent the standard deviation for triplicate quantitative real-time RT-PCR analyses. DNA methylation levels and mRNA expression levels on days 3 (AZA3) and 6 (AZA6) were compared with those of untreated cells (AZA0). After 5-aza-dC treatment, reduction of DNA methylation levels and restoration of the mRNA expression levels of *ADCY5* (**A**), *EVX1* (**B**) and *TBX20* (**E**) were observed in both of the cell lines used. In panel **C**, since reduction of the DNA methylation level was not induced by 5-aza-dC in PC9 cells, restoration of mRNA expression did not occur in these cells. Panel **D** shows reduction of the DNA methylation level and restoration of the mRNA expression level in PC9 cells.
doi:10.1371/journal.pone.0059444.g003

### Silencing of Recurrence-related Genes due to DNA Hypermethylation

Among the 28 genes listed in Table 1, we further focused on 6 genes (*ADCY5* [20,21], *CNTNAP2* [22,23], *EVX1* [24], *GFRA1* [25], *PDE9A* [26,27] and *TBX20* [28]) for which implications in transcription regulation, apoptosis or cell adhesion had been reported. Quantitative real-time RT-PCR analysis of these 6 genes was performed in 132 N and 151 T samples for which total RNA was available. mRNA expression levels for the *ADCY5, EVX1, GFRA1, PDE9A* and *TBX20* genes in T samples were significantly lower than those in N samples, although the reduced expression of the *CNTNAP2* gene did not reach statistical significance (Figure 2B). The DNA methylation statuses (β-values in N and T samples) of the 6 genes are also shown in Figure 2A; the data suggested that DNA hypermethylation of these genes might result in reduction of mRNA expression in tissue samples from the same cohort.

DNA methylation levels of the *ADCY5, EVX1, GFRA1, PDE9A* and *TBX20* genes in lung cancer cell lines A549, PC9, VMRC-LCD and EBC-1 are shown in Figure S2. To examine the effects of the DNA methylation inhibitor, the top two cell lines showing the highest DNA methylation levels (β-values) were selected for each gene. In fact, mRNA expression levels determined by quantitative real-time RT-PCR analysis of the genes (with the exception of PDE9A) were extremely low in the cell lines selected. 5-aza-dC treatment induced marked reduction of DNA methylation levels and restored the mRNA expression levels of *ADCY5, EVX1, GFRA1* and *TBX20* (Figure 3). With regard to *GFRA1*, since reduction of the DNA methylation level was not induced by 5-aza-dC, restoration of mRNA expression did not occur in PC9 cells. Taken together with Figures 2 and 3, the data suggested that the examined genes were silenced due to DNA hypermethylation in the lung cancers. With regard to *PDE9A*, for which the mRNA expression levels were high even in the top two cell lines showing the highest levels of DNA methylation, 5-aza-dC treatment did not further increase the mRNA expression level in the two cell lines. The PC9 cells were then additionally treated with 5-aza-dC, and restoration of *PDE9A* mRNA expression due to DNA demethylation was confirmed in the cells (Figure 3).

### Clinicopathological Impact of Reduced Expression of mRNA for Recurrence-related Genes

Reduced expression of mRNA for *ADCY5, EVX1, GFRA1* and *PDE9A* in T samples was correlated with clinicopathological parameters reflecting tumor aggressiveness, such as a larger tumor diameter, higher histological grade, blood vessel invasion, pleural invasion and tumor anthracosis (Table 2), although their mRNA expression levels were not predictors of recurrence that were independent of known parameters such as pathological-TNM stage and lymph node metastasis (Table S4). With regard to the correlation with histological subtype, levels of mRNA expression for *GFRA1* and *PDE9A* were significantly higher in lepidic-type LADCs showing a less invasive growth pattern than in other histological subtypes.

## Discussion

The 'field cancerization' phenomenon in the lung has become evident, being especially associated with cigarette smoking [31]. We and other groups have reported DNA methylation of specific genes or chromosomal loci in non-cancerous lung tissue obtained from lung cancer patients, or in lung tissue from cancer-free smokers [8–10]. These previous data drew our attention to DNA methylation alterations at precancerous stages of LADC. However, the impact of DNA methylation alterations at precancerous stages on the expression of specific gene and clinicopathological parameters of established cancers has remained unclear. Moreover, previous examinations focusing on precancerous stages in the lung have not involved a genome-wide approach. Although Selamat et al. and Lockwood et al. have reported Infinium assay results for 59 and 43 lung cancer samples, respectively [16,17], they did not focus on precancerous stages.

Here we have reported the results of the Infinium assay for 326 lung tissue samples including 145 N samples. Our cumulative logit model analysis revealed stepwise progression of DNA methylation alterations from C to N, and then T samples on 3,270 probes. Genome-wide analysis at single-CpG resolution confirmed that DNA methylation alterations actually occurred even at precancerous stages, although the possibility that such alterations observed in N samples had been influenced by differences in tissue composition between C and N samples cannot be completely excluded. Moreover, it was clearly shown that such DNA methylation alterations had clinicopathological impact, since many probes in N samples were significantly correlated with recurrence after establishment of LADCs (Figure 1B). DNA methylation profiles determining outcome are already established at precancerous stages. The finding that the number of probes showing DNA methylation alterations significantly associated with recurrence in N samples was larger than that in T samples may have been due to the fact that passenger DNA methylation alterations occurring during progression from the precancerous stages to established cancers may have masked any clinicopathologically significant DNA methylation profiles in T samples.

Next, we focused on 28 recurrence-related genes that are normally unmethylated and for which DNA hypermethylation in N samples was strengthened in T samples (Table 1). Among these 28 genes, we further focused on *ADCY5, CNTNAP2, EVX1, GFRA1, PDE9A* and *TBX20*, based on their previously reported implications in transcription regulation, apoptosis or cell adhesion. (a) The data in *adcy5*-knockout mice indicated that ADCY5 promotes apoptosis in cardiomyocytes [20,21]. Although large-scale screening studies of leukemias have identified *ADCY5* as one of the genes that are methylated in leukemic cells [32,33], the clinicopathological impact of DNA methylation of the *ADCY5* gene has not yet been clarified in human malignancies. (b) CNTNAP2, a glial adhesion molecule, binds extracellularly to contactin 2, an immunoglobulin superfamily neural recognition protein [22]. *CNTNAP2* is known to be a tumor-suppressor gene for gliomas, and is disrupted by chromosomal translocations and gene mutations [23]. Although a large-scale screening study of

**Table 2.** Correlation between mRNA expression levels of recurrence-related genes and clinicopathological factors.

| Clinicopathological parameters | Number of tumors | *ADCY5* | | *EVX1* | | *GFRA1* | | *PDE9A* | | *TBX20* | |
|---|---|---|---|---|---|---|---|---|---|---|---|
| | | Expression[a] | $P^b$ | Expression[a] | $P^b$ | Expression[a] | $P^b$ | Expression[a] | $P^b$ | Expression[a] | $P^b$ |
| Tumor diameter | | | | | | | | | | | |
| <2.5 cm | 43 | −4.95±2.10 | $1.63\times10^{-1}$[c] | −2.80±1.82 | $4.24\times10^{-1}$[c] | −3.27±2.67 | $1.60\times10^{-3}$[c] | 0.50±1.39 | $3.40\times10^{-2}$[c] | −5.73±2.68 | $7.65\times10^{-1}$[c] |
| ≥2.5 cm, <4 cm | 61 | −5.25±2.39 | | −2.36±2.16 | | −4.02±2.86 | | 0.28±1.76 | | −5.76±2.78 | |
| ≥4 cm | 47 | −6.14±2.76 | | −3.04±2.02 | | −5.74±3.28 | | −0.50±1.59 | | −6.10±2.84 | |
| Histological subtype[d] | | | | | | | | | | | |
| Lepidic | 12 | −4.19±1.61 | $2.10\times10^{-1}$[c] | −2.73±2.14 | $1.79\times10^{-1}$[c] | −1.64±2.35 | $1.71\times10^{-4}$[c] | 0.93±1.07 | $1.73\times10^{-3}$[c] | −6.24±1.79 | $1.28\times10^{-1}$[c] |
| Acinar | 24 | −6.03±2.01 | | −2.91±2.09 | | −5.41±2.72 | | −0.20±1.36 | | −5.77±2.57 | |
| Papillary | 69 | −5.30±2.35 | | −2.29±1.99 | | −3.90±2.65 | | 0.23±1.63 | | −5.28±2.80 | |
| Micropapillary | 15 | −4.69±2.19 | | −2.35±2.10 | | −3.47±2.87 | | 1.20±1.27 | | −6.89±1.79 | |
| Solid | 28 | −6.34±3.24 | | −3.62±1.88 | | −6.27±3.62 | | −0.91±1.81 | | −6.37±3.11 | |
| Invasive mucinous | 3 | −4.64±1.46 | | −3.19±1.24 | | −2.95±1.43 | | 0.16±1.68 | | −8.21±0.14 | |
| Histological grades | | | | | | | | | | | |
| G1 | 56 | −4.60±1.80 | $1.28\times10^{-3}$[c] | −2.68±1.90 | $4.57\times10^{-2}$[c] | −2.62±1.93 | $4.80\times10^{-10}$ | 0.55±1.41 | $1.32\times10^{-4}$ | −5.48±2.69 | $9.50\times10^{-2}$ |
| G2 | 65 | −5.58±2.33 | | −2.32±2.10 | | −4.59±2.71 | | 0.25±1.57 | | −5.74±2.67 | |
| G3 | 30 | −6.73±3.20 | | −3.54±1.92 | | −7.01±3.60 | | −1.06±1.77 | | −6.81±2.94 | |
| Lymphatic invasion | | | | | | | | | | | |
| Negative | 52 | −5.31±2.43 | 1.00[e] | −2.76±1.71 | 1.00[e] | −3.95±3.38 | 1.00[e] | 0.06±1.64 | 1.00[e] | −5.86±2.42 | $9.82\times10^{-1}$[e] |
| Positive | 99 | −5.52±2.50 | | −2.66±2.19 | | −4.55±2.92 | | 0.12±1.67 | | −5.85±2.93 | |
| Blood vessel invasion | | | | | | | | | | | |
| Negative | 43 | −4.89±2.40 | $2.38\times10^{-1}$[e] | −2.77±1.84 | $7.68\times10^{-1}$[e] | −3.13±3.45 | $2.81\times10^{-2}$[e] | 0.63±1.68 | $6.39\times10^{-2}$[e] | −5.71±2.60 | 1.00[e] |
| Positive | 108 | −5.66±2.47 | | −2.67±2.11 | | −4.82±2.81 | | −0.11±1.60 | | −5.92±2.83 | |
| Pleural invasion | | | | | | | | | | | |
| Negative | 78 | −5.16±2.42 | $4.45\times10^{-1}$[c] | −2.77±2.15 | $4.60\times10^{-1}$[c] | −3.65±2.83 | $7.28\times10^{-3}$[c] | 0.28±1.61 | $5.82\times10^{-1}$[c] | −5.95±2.51 | $5.38\times10^{-1}$[c] |
| Invasion to the visceral pleura beyond the elastic fiber | 33 | −5.88±2.68 | | −2.62±2.07 | | −4.99±3.54 | | 0.03±1.93 | | −6.41±2.96 | |
| Invasion to the surface of the visceral pleura | 22 | −4.96±2.07 | | −2.16±1.62 | | −4.01±2.66 | | 0.18±1.29 | | −4.98±2.82 | |
| Invasion to the parietal pleura | 18 | −6.47±2.49 | | −3.15±1.90 | | −6.56±2.71 | | −0.65±1.58 | | −5.52±3.22 | |
| Tumor anthracosis [f] | | | | | | | | | | | |
| Negative | 68 | −4.97±2.57 | $8.27\times10^{-2}$[e] | −2.37±2.22 | $2.04\times10^{-1}$[e] | −3.32±2.80 | $1.08\times10^{-3}$[e] | 0.70±1.46 | $1.66\times10^{-4}$[e] | −5.51±2.78 | $1.99\times10^{-1}$[e] |
| Positive | 82 | −5.87±2.30 | | −2.91±1.79 | | −5.10±3.02 | | −0.39±1.66 | | −6.09±2.69 | |

[a]Average of log2-transformed mRNA expression levels/GAPDH ± standard deviation. [b]Adjusted *P*-values using adjusted Bonferroni correction. [c]Analysis of variance between groups. [d]Predominant histological subtypes of LADCs were diagnosed according to the classification devised by the International Association for the Study of Lung Cancer, the American Thoracic Society and the European Respiratory Society [29]. [e]Welch's T-test. [f]Coal dust is accumulated in active fibroblast proliferation foci, which is associated with poorer prognosis of lung adenocarcinoma patients and reflects an active cancer-stromal interaction [30]. *P* values of <0.05 are underlined.

doi:10.1371/journal.pone.0059444.t002

pancreatic cancers has identified *CNTNAP2* as one of the genes that are methylated in cancer cells [34], the clinicopathological impact of DNA methylation of the *CNTNAP2* gene has not yet been elucidated in human malignancies. (c) *EVX1*, encoding a homeobox protein, functions as a potent repressor of gene transcription and plays an important role during mouse embryogenesis [24]. Although Truong et al. have recently suggested that DNA hypermethylation of the *EVX1* gene may be a predictor of recurrence of prostatic cancers [35], the implications of *EVX1* in human cancers other than prostatic cancer have been unclear. (d) GFRA1 is a receptor for glial cell-derived neurotrophic factor (GDNF) and enriched in the pre- and post-synaptic compartments. GDNF triggers trans-homophilic binding between GFRA1 molecules, resulting in adhesion between *GFRA1*-expressing cells [25]. Overexpression of *GFRA1* has been reported in chemotherapy-sensitive oligodendrogliomas [36]. Although Salamat et al. described *GFRA1* as one of the genes differentially methylated between cancerous and non-cancerous tissue obtained from lung cancer patients subclustered on the basis of DNA methylation profiles [16], the clinicopathological impact of DNA methylation of the *GFRA1* gene was not examined in LADCs. (e) *PDE9A* encodes cGMP-specific phosphodiesterase [26]. PDE9A inhibitor has been reported to induce apoptosis of breast cancer cell lines through caspase 3 activation [27]. On the other hand, breakpoints within the *PDE9A* gene have been frequently observed in B-cell precursor acute lymphoblastic leukemia [36]. However, the implications of DNA methylation in the regulation of *PDE9A* have never been reported in human malignancies or other diseases. (f) TBX20, a member of the T-box transcription factors, is a critical regulator of heart development, and mutations of the human *TBX20* gene result in cardiac malformations [28]. However, the implications of DNA methylation in *TBX20* regulation and of *TBX20* dysfunction in human malignancies have never been reported.

Among these 6 genes, DNA hypermethylation of the *ADCY5, EVX1, GFRA1, PDE9A* and *TBX20* genes was associated with reduced mRNA expression in tissue samples of the same cohort. 5-aza-dC treatment of human lung cancer cell lines restored the expression of the 5 genes, indicating that genes showing DNA hypermethylation at precancerous stages are actually silenced due to DNA hypermethylation during lung carcinogenesis. With regard to *PDE9A*, the level of mRNA expression was not necessarily low and was not always restored by 5-aza-dC treatment in any of the cell lines examined, indicating that DNA methylation is not the only mechanism responsible for *PDE9A* regulation in lung cancers. In addition, there are gaps between the timing of the reduction of DNA methylation and recovery of mRNA expression in *ADCY5* in EBC-1 cells and A549 cells and *GFRA1* in EBC-1 cells, again indicating the possibility that there are alternative mechanisms regulating the mRNA expression levels of these genes other than DNA methylation. Reduced expression of the mRNAs for the *ADCY5, EVX1, GFRA1* and *PDE9A* genes was significantly correlated with clinicopathological parameters (Table 2), indicating that DNA methylation alterations, even from the precancerous stage, ultimately determine the tumor phenotype through gene silencing.

Unlike the present study, which was conducted to clarify the significance of DNA methylation alterations at precancerous stages, many previous studies attempted to establish prognostic factors based on DNA methylation status using candidate gene approaches [37–41]. Microarray studies are generally considered to be useful for establishing prognostic biomarkers. In lung cancers, array-based DNA methylation screening [42] has been performed for prognostication. Next-generation sequencing associated with bioinformatics analysis [43] has also been reported for lung cancers. Such previous studies identified the *RASSF1A* [37], *PITX2* [38], *SHOX2* [38], *TFPI-2* [39], *FHIT* [40], *p16* [41], *CDH13* [41], and *APC* [41] genes as predictors of recurrence of lung cancers. The genes for which DNA methylation status at precancerous stages ($\beta_N$ values) was associated with recurrence in the present study are different from the prognostic biomarkers selected in previous studies based on the DNA methylation status of tumorous tissues themselves.

In summary, DNA methylation status is not simply altered at precancerous stages, and is significantly correlated with recurrence after establishment of LADCs. DNA methylation alterations at precancerous stages are strengthened in comparison to normal lung tissues during progression to established LADC. DNA methylation profiles at precancerous stages may determine tumor aggressiveness through alterations in the expression of mRNAs for specific genes.

## Supporting Information

**Figure S1 Verification of the results of the Infinium assay using pyrosequencing methods.** To overcome the PCR bias in pyrosequencing, the PCR conditions were optimized for each primer set, as described previously (Nagashio R, et al. Int J Cancer 129:1170, 2011). Pyrosequencing was performed for the *CNTNAP2, EVX1, GFRA1, PDE9A* and *TBX20* genes using 9 representative T samples and 9 corresponding N samples. β-values obtained from the Infinium assay were strongly correlated with DNA methylation levels obtained by pyrosequencing in all 5 genes, indicating that the results of the Infinium assay were successfully verified.
(TIF)

**Figure S2 DNA methylation levels for the *ADCY5, EVX1, GFRA1, PDE9A* and *TBX20* genes in lung cancer cell lines.** DNA methylation levels (β-values) for the *ADCY5, EVX1, GFRA1, PDE9A* and *TBX20* genes in all 4 of the lung cancer cell lines were examined by Infinium assay. To examine the effects of the DNA methylation inhibitor, 5-aza-2′-deoxycytidine, the top two cell lines showing the highest DNA methylation levels were selected for each gene: EBC-1 and A549 cells for the *ADCY5* gene, VMRC-LCD and EBC-1 cells for the *EVX1* gene, EBC-1 and PC9 cells for the *GFRA1* gene, VMRC-LCD and A549 cells for the *PDE9A* gene, and EBC-1 and PC9 cells for the *TBX20* gene.
(TIF)

**Table S1 Characteristics of the lung cancer cell lines.**
(PDF)

**Table S2 Probe ID and primer sequences for quantitative real-time reverse transcription-PCR.**
(PDF)

**Table S3 The probes for which call proportions in all examined tissue samples were less than 90%.**
(PDF)

**Table S4 Multivariate analysis of clinicopathological parameters and mRNA expression levels of selected genes associated with recurrence in patients with lung adenocarcinomas.**
(PDF)

## Acknowledgments

The authors thank Y. Shimada for providing technical assistance.

## Author Contributions

Conceived and designed the experiments: EA YK. Performed the experiments: TS EA TK. Analyzed the data: TS EA KS TB YK. Contributed reagents/materials/analysis tools: EA KT SW YK. Wrote the paper: TS EA YK.

## References


1. Pao W, Girard N (2011) New driver mutations in non-small-cell lung cancer. Lancet Oncol 12: 175–180.
2. Greulich H (2010) The genomics of lung adenocarcinoma: opportunities for targeted therapies. Genes Cancer 1: 1200–1210.
3. Liu P, Morrison C, Wang L, Xiong D, Vedell P, et al. (2012) Identification of somatic mutations in non-small cell lung carcinomas using whole-exome sequencing. Carcinogenesis 33: 1270–1276.
4. Baylin SB, Jones PA (2011) A decade of exploring the cancer epigenome-biological and translational implications. Nat Rev Cancer 11: 726–734.
5. Kanai Y (2010) Genome-wide DNA methylation profiles in precancerous conditions and cancers. Cancer Sci 101: 36–45.
6. Kanai Y (2008) Alterations of DNA methylation and clinicopathological diversity of human cancers. Pathol Int 58: 544–558.
7. Kanai Y, Hirohashi S (2007) Alterations of DNA methylation associated with abnormalities of DNA methyltransferases in human cancers during transition from a precancerous to a malignant state. Carcinogenesis 28: 2434–2442.
8. Heller G, Zielinski CC, Zöchbauer-Müller S (2010) Lung cancer: from single-gene methylation to methylome profiling. Cancer Metastasis Rev 29: 95–107.
9. Hamilton JP (2011) Epigenetics: principles and practice. Dig Dis. 29: 130–135.
10. Eguchi K, Kanai Y, Kobayashi K, Hirohashi S (1997) DNA hypermethylation at the D17S5 locus in non-small cell lung cancers: its association with smoking history. Cancer Res 57: 4913–4915.
11. Zöchbauer-Müller S, Lam S, Toyooka S, Virmani AK, Toyooka KO, et al. (2003) Aberrant methylation of multiple genes in the upper aerodigestive tract epithelium of heavy smokers. Int J Cancer 107: 612–616.
12. Arai E, Chiku S, Mori T, Gotoh M, Nakagawa T, et al. (2012) Single-CpG-resolution methylome analysis identifies clinicopathologically aggressive CpG island methylator phenotype clear cell renal cell carcinomas. Carcinogenesis 33: 1487–1493.
13. Arai E, Ushijima S, Fujimoto H, Hosoda F, Shibata T, et al. (2009) Genome-wide DNA methylation profiles in both precancerous conditions and clear cell renal cell carcinomas are correlated with malignant potential and patient outcome. Carcinogenesis 30: 214–221.
14. Arai E, Kanai Y, Ushijima S, Fujimoto H, Mukai K, et al. (2006) Regional DNA hypermethylation and DNA methyltransferase (DNMT) 1 protein overexpression in both renal tumors and corresponding nontumorous renal tissues. Int J Cancer 119: 288–296.
15. Bibikova M, Le J, Barnes B, Saedinia-Melnyk S, Zhou L, et al. (2009) Genome-wide DNA methylation profiling using Infinium® assay. Epigenomics 1: 177–200.
16. Selamat SA, Chung BS, Girard L, Zhang W, Zhang Y, et al. (2012) Genome-scale analysis of DNA methylation in lung adenocarcinoma and integration with mRNA expression. Genome Res 22: 1197–1211.
17. Lockwood WW, Wilson IM, Coe BP, Chari R, Pikor LA, et al. (2012) Divergent genomic and epigenomic landscapes of lung cancer subtypes underscore the selection of different oncogenic pathways during tumor development. PLoS One 7: e37775.
18. Travis WD, Brambilla E, Müller-Hermelink HK, Harris CC (2004) World Health Organization Classification of Tumours. Pathology and Genetics of Tumours of the Lung, Pleura, Thymus and Heart. Lyon: IARC Press. pp. 35–44.
19. Sambrook J, Fritsch EF, Maniatis T (1989) Molecular Cloning. A Laboratory Manual (2nd ed). Cold spring Harbor: Cold Spring Harbor Laboratory Press. pp. E3–E4.
20. Yan L, Vatner DE, O'Connor JP, Ivessa A, Ge H, et al. (2007) Type 5 adenylyl cyclase disruption increases longevity and protects against stress. Cell 130: 247–258.
21. Okumura S, Vatner DE, Kurotani R, Bai Y, Gao S, et al. (2007) Disruption of type 5 adenylyl cyclase enhances desensitization of cyclic adenosine monophosphate signal and increases Akt signal with chronic catecholamine stress. Circulation 116: 1776–1783.
22. Poliak S, Salomon D, Elhanany H, Sabanay H, Kiernan B, et al. (2003) Juxtaparanodal clustering of Shaker-like K+ channels in myelinated axons depends on Caspr2 and TAG-1. J Cell Biol 162: 1149–1160.
23. Bralten LB, Gravendeel AM, Kloosterhof NK, Sacchetti A, Vrijenhoek T, et al. (2010) The CASPR2 cell adhesion molecule functions as a tumor suppressor gene in glioma. Oncogene 29: 6138–6148.
24. Briata P, Van De Werken R, Airoldi I, Ilengo C, Di Blas E, et al. (1995) Transcriptional repression by the human homeobox protein EVX1 in transfected mammalian cells. J Biol Chem 270: 27695–27701.
25. Ledda F, Paratcha G, Sandoval-Guzmán T, Ibáñez CF (2007) GDNF and GFRalpha1 promote formation of neuronal synapses by ligand-induced cell adhesion. Nat Neurosci 10: 293–300.
26. Fisher DA, Smith JF, Pillar JS, St Denis SH, Cheng JB (1998) Isolation and characterization of PDE9A, a novel human cGMP-specific phosphodiesterase. J Biol Chem 273: 15559–15564.
27. Saravani R, Karami-Tehrani F, Hashemi M, Aghaei M, Edalat R (2012) Inhibition of phosphodiesterase 9 induces cGMP accumulation and apoptosis in human breast cancer cell lines, MCF-7 and MDA-MB-468. Cell Prolif 45: 199–206.
28. Chakraborty S, Yutzey KE (2012) Tbx20 regulation of cardiac cell proliferation and lineage specialization during embryonic and fetal development in vivo. Dev Biol 363: 234–246.
29. Travis WD, Brambilla E, Noguchi M, Nicholson AG, Geisinger KR, et al. (2011) International association for the study of lung cancer/American thoracic society/European respiratory society international multidisciplinary classification of lung adenocarcinoma. J Thorac Oncol 6: 244–285.
30. Noguchi M, Morikawa A, Kawasaki M, Matsuno Y, Yamada T, et al. (1995) Small adenocarcinoma of the lung. Histologic characteristics and prognosis. Cancer 75: 2844–2852.
31. Kadara H, Kabbout M, Wistuba II (2012) Pulmonary adenocarcinoma: a renewed entity in 2011. Respirology 17: 50–65.
32. Kuang SQ, Tong WG, Yang H, Lin W, Lee MK, et al. (2008) Genome-wide identification of aberrantly methylated promoter associated CpG islands in acute lymphocytic leukemia. Leukemia 22: 1529–1538.
33. Tong WG, Wierda WG, Lin E, Kuang SQ, Bekele BN, et al. (2010) Genome-wide DNA methylation profiling of chronic lymphocytic leukemia allows identification of epigenetically repressed molecular pathways with clinical impact. Epigenetics 5: 499–508.
34. Omura N, Li CP, Li A, Hong SM, Walter K, et al. (2008) Genome-wide profiling of methylated promoters in pancreatic adenocarcinoma. Cancer Biol Ther 7: 1146–1156.
35. Truong M, Yang B, Wagner J, Kobayashi Y, Rajamanickam V, et al. (2012) Even-skipped homeobox 1 is frequently hypermethylated in prostate cancer and predicts PSA recurrence. Br J Cancer 107: 100–107.
36. Sinclair PB, Parker H, An Q, Rand V, Ensor H, et al. (2011) Analysis of a breakpoint cluster reveals insight into the mechanism of intrachromosomal amplification in a lymphoid malignancy. Hum Mol Genet 20: 2591–2602.
37. de Fraipont F, Levallet G, Creveuil C, Bergot E, Beau-Faller M, et al. (2012) An apoptosis methylation prognostic signature for early lung cancer in the IFCT-0002 trial. Clin Cancer Res 18: 2976–2986.
38. Dietrich D, Hasinger O, Liebenberg V, Field JK, Kristiansen G, et al. (2012) DNA methylation of the homeobox genes PITX2 and SHOX2 predicts outcome in non-small-cell lung cancer patients. Diagn Mol Pathol 21: 93–104.
39. Wu D, Xiong L, Wu S, Jiang M, Lian G, et al. (2012) TFPI-2 methylation predicts poor prognosis in non-small cell lung cancer. Lung Cancer 76: 106–111.
40. Verri C, Roz L, Conte D, Liloglou T, Livio A, et al. (2009) Fragile histidine triad gene inactivation in lung cancer: the European Early Lung Cancer project. Am J Respir Crit Care Med 179: 396–401.
41. Brock MV, Hooker CM, Ota-Machida E, Han Y, Guo M, et al. (2008) DNA methylation markers and early recurrence in stage I lung cancer. N Engl J Med 358: 1118–1128.
42. Morán A, Fernández-Marcelo T, Carro J, De Juan C, Pascua I, et al. (2012) Methylation profiling in non-small cell lung cancer: clinical implications. Int J Oncol 40: 739–746.
43. Carvalho RH, Haberle V, Hou J, van Gent T, Thongjuea S, et al. (2012) Genome-wide DNA methylation profiling of non-small cell lung carcinomas. Epigenetics Chromatin 5: 9.

**Carcinogenesis** vol.33 no.8 pp.1487–1493, 2012
doi:10.1093/carcin/bgs177
*Advance Access Publication May 18, 2012*

# Single-CpG-resolution methylome analysis identifies clinicopathologically aggressive CpG island methylator phenotype clear cell renal cell carcinomas

**Eri Arai[1], Suenori Chiku[2], Taisuke Mori[1], Masahiro Gotoh[1], Tohru Nakagawa[3], Hiroyuki Fujimoto[3] and Yae Kanai[1,*]**

[1]Division of Molecular Pathology, National Cancer Center Research Institute, Tokyo 104-0045, Japan, [2]Science Solutions Division, Mizuho Information and Research Institute, Inc., Tokyo 101-8443, Japan and [3]Department of Urology, National Cancer Center Hospital, Tokyo 104-0045, Japan

*To whom correspondence should be addressed. Tel: +81 3 3542 2511; Fax: +81 3 3248 2463;
Email: ykanai@ncc.go.jp

**To clarify the significance of DNA methylation alterations during renal carcinogenesis, methylome analysis using single-CpG-resolution Infinium array was performed on 29 normal renal cortex tissue (C) samples, 107 non-cancerous renal cortex tissue (N) samples obtained from patients with clear cell renal cell carcinomas (RCCs) and 109 tumorous tissue (T) samples. DNA methylation levels at 4830 CpG sites were already altered in N samples compared with C samples. Unsupervised hierarchical clustering analysis based on DNA methylation levels at the 801 CpG sites, where DNA methylation alterations had occurred in N samples and were inherited by and strengthened in T samples, clustered clear cell RCCs into Cluster A ($n$ = 90) and Cluster B ($n$ = 14). Clinicopathologically aggressive tumors were accumulated in Cluster B, and the cancer-free and overall survival rates of patients in this cluster were significantly lower than those of patients in Cluster A. Clear cell RCCs in Cluster B were characterized by accumulation of DNA hypermethylation on CpG islands and considered to be CpG island methylator phenotype (CIMP)-positive cancers. DNA hypermethylation of the CpG sites on the FAM150A, GRM6, ZNF540, ZFP42, ZNF154, RIMS4, PCDHAC1, KHDRBS2, ASCL2, KCNQ1, PRAC, WNT3A, TRH, FAM78A, ZNF671, SLC13A5 and NKX6-2 genes became hallmarks of CIMP in RCCs. On the other hand, Cluster A was characterized by genome-wide DNA hypomethylation. These data indicated that DNA methylation alterations at precancerous stages may determine tumor aggressiveness and patient outcome. Accumulation of DNA hypermethylation on CpG islands and genome-wide DNA hypomethylation may each underlie distinct pathways of renal carcinogenesis.**

## Introduction

Clear cell renal cell carcinoma (RCC) is the most common histological subtype of adult kidney cancer and frequently affects working-age adults in midlife. In general, RCCs at an early stage are curable by nephrectomy. However, some RCCs relapse and metastasize to distant organs, even if the resection has been considered complete (1). Such clinicopathological diversity may be attributable to distinct pathways of renal carcinogenesis (2). It is well known that clear cell RCCs are characterized by inactivation of the Von Hippel–Lindau tumor-suppressor gene (3). In addition, systematic resequencing and exome analysis of RCCs are now being performed by The Cancer Genome Atlas (4), The Cancer Genome Project (5) and other international efforts (6). Such efforts have revealed that renal carcinogenesis involves inactivation of histone-modifying genes, such as SETD2 (7), a histone H3 lysine 36 methyltransferase, JARIDIC (KDM5C (7)), a histone H3 lysine 4 demethylase, and UTX (KMD6A (8)), a histone H3 lysine 27 demethylase, as well as the SWI/SNF chromatin-remodeling complex gene, PBRM1 (9). Non-synonymous mutations of the NF2 gene and truncating mutations of the MLL2 gene have also been reported (7). However, such gene mutations cannot fully explain the clinicopathological diversity of clear cell RCCs.

Not only genetic, but also epigenetic events appear to accumulate during carcinogenesis, and both types of event reflect the clinicopathological diversity of cancers in various organs in association with each other (10–12). DNA methylation alterations are one of the most consistent epigenetic changes in human cancers (13–16). In fact, on the basis of methylation-specific PCR (MSP), combined bisulfite restriction enzyme analysis (17,18) and bacterial artificial chromosome array-based methylated CpG island amplification (BAMCA (19,20)), we have suggested that non-cancerous renal cortex tissue obtained from patients with RCCs is already at the precancerous stage associated with DNA methylation alterations, even though no remarkable histological changes are evident and there is no association with chronic inflammation or persistent infection with viruses or other pathogenic microorganisms. Genome-wide analysis using BAMCA revealed that DNA methylation status in non-cancerous renal cortex tissue at the precancerous stage was basically inherited by the corresponding clear cell RCC in individual patients (19). DNA methylation alterations at the precancerous stage may confer further susceptibility to genetic and epigenetic alterations and generate more malignant clear cell RCCs (2,13). However, in our previous studies using BAMCA, the resolution and the number of probes were limited. Therefore, further analysis is needed to clarify the significance of DNA methylation alterations in renal carcinogenesis.

Recently, methylome analysis using the Infinium array has made it possible to interrogate 27 000 highly informative CpG sites at single-CpG resolution (21). In order to clarify the significance of DNA methylation alterations during renal carcinogenesis, we used the Infinium BeadChip system to perform genome-wide DNA methylation analysis of 29 samples of normal renal cortex tissue (C) obtained from patients without any primary renal tumors, 107 samples of non-cancerous renal cortex tissue (N) from patients with clear cell RCCs and 109 samples of tissue from the tumors (T) themselves. Correlations between the genome-wide DNA methylation profiles and clinicopathological parameters were then examined.

**Abbreviations:** BAMCA, bacterial artificial chromosome array-based methylated CpG island amplification; C, normal renal cortex tissue obtained from patients without any primary renal tumor; CIMP, CpG island methylator phenotype; HCC, hepatocellular carcinoma; N, non-cancerous renal cortex tissue obtained from patients with clear cell renal cell carcinomas; NCBI, National Center for Biotechnology Information; RCC, renal cell carcinoma; T, tumorous tissue; TNM, Tumor-Node-Metastasis.

## Materials and methods

*Patients and tissue samples*

The 109 T samples and corresponding 107 N samples showing no remarkable histological changes were obtained from materials that had been surgically resected from 110 patients with primary clear cell RCCs. These patients did not receive preoperative treatment and underwent nephrectomy at the National Cancer Center Hospital, Tokyo, Japan. There were 79 men and 31 women with a mean (±SD) age of 62.8 ± 10.3 years (range 36–85 years). Histological diagnosis was made in accordance with the World Health Organization classification (22) (Supplementary Figure S1, available at *Carcinogenesis* Online). All the tumors were graded on the basis of criteria described previously (23) and classified according to the pathological Tumor-Node-Metastasis (TNM) classification (24). The criteria for macroscopic configuration of RCC (17–19) followed those established for hepatocellular carcinoma (HCC): type 3 (contiguous multinodular type) HCCs show poorer histological differentiation and a higher incidence of intrahepatic metastasis than type 1 (single nodular type) and type 2 (single nodular type with extranodular growth) HCCs (25). The presence or absence of vascular involvement was examined microscopically on slides stained with hematoxylin–eosin and elastica van Gieson. The presence or absence of tumor thrombi in the main trunk of the renal vein was examined macroscopically.

RCC is usually enclosed by a fibrous capsule and well demarcated, and hardly ever contains fibrous stroma between cancer cells. Therefore, we were able to obtain cancer cells from surgical specimens, avoiding contamination with both non-cancerous epithelial cells and stromal cells.

For comparison, 29 samples of normal renal cortex tissue (C1–C29) were obtained from materials that had been surgically resected from 29 patients without any primary renal tumor. These patients included 18 men and 11 women with a mean (±SD) age of 61.4± 10.8 years (range 31–81 years). Of these patients, 22 had undergone nephroureterectomy for urothelial carcinomas of the renal pelvis and ureter, 6 had undergone nephrectomy with resection of retroperitoneal sarcoma around the kidney, and the remaining 1 had undergone paraaortic lymph node dissection for metastatic germ cell tumor, which resulted in simultaneous nephrectomy because it was not possible to preserve the renal artery.

All patients included in this study provided written informed consent, and the study was approved by the Ethics Committee of the National Cancer Center, Tokyo, Japan.

*Infinium assay*

High-molecular-weight DNA from fresh frozen tissue samples was extracted using phenol–chloroform, followed by dialysis (26). Five-hundred-nanogram aliquots of DNA were subjected to bisulfite conversion using an EZ DNA Methylation-Gold™ Kit (Zymo Research, Irvine, CA). Subsequently DNA methylation status at 27 578 CpG loci was examined at single-CpG resolution using the Infinium HumanMethylation27 Bead Array (Illumina, San Diego, CA). This array contains CpG sites located within the proximal promoter regions of the transcription start sites of 14 475 consensus coding sequences in the National Center for Biotechnology Information Database. On average, two assays were selected per gene, and from 3 to 20 CpG sites for more than 200 cancer-related and imprinted genes. Forty control probes were employed for each array; these included staining, hybridization, extension, bisulfite conversion and negative controls. An Evo robot (Tecan, Switzerland) was used for automated sample processing. Whole-genome amplification was performed using the Infinium Assay Kit (Illumina (21)). After hybridization, the specifically hybridized DNA was fluorescence labeled by a single-base extension reaction and detected using a BeadScan reader (Illumina) in accordance with the manufacturer's protocols. The data were then assembled using GenomeStudio methylation software (Illumina). At each CpG site, the ratio of the fluorescent signal was measured using a methylated probe relative to the sum of the methylated and unmethylated probes, i.e. the so-called $\beta$-value, which ranges from 0.00 to 1.00, reflecting the methylation level of an individual CpG site.

*Statistics*

In the Infinium assay, the call proportions (*P*-values for detection of signals above the background <0.01) for 32 probes (shown in Supplementary Table S1, available at *Carcinogenesis* Online) in all of the tissue samples examined were less than 90%. Since such a low proportion may be attributable to polymorphism at the probe CpG sites, these 32 probes were excluded from the present assay. In addition, all CpG sites on chromosomes X and Y were excluded, to avoid any gender-specific methylation bias, leaving a final total of 26 454 autosomal CpG sites.

Infinium probes showing significant differences in DNA methylation levels between the 29 C and 107 N samples were identified by a logistic model adjusted by sex, age and experimental batch. Ordered differences from 29 C to 107 N and then to 109 T samples themselves were examined by the cumulative logit model adjusted by sex, age and experimental batch. Differences of DNA methylation status between 104 paired samples of N and the corresponding T obtained from a single patient and assayed in the same experimental batch were examined by Wilcoxon matched pairs test. A false discovery rate (FDR) of $q = 0.01$ was considered significant. Unsupervised hierarchical clustering (Euclidan distance, Ward method) based on DNA methylation levels ($\Delta\beta_{T-N}$) was performed in patients with clear cell RCCs. Correlations between clusters of patients and clinicopathological parameters were examined using Wilcoxon rank sum test and Fisher's exact test. Survival curves of patients belonging to each cluster were calculated by the Kaplan–Meier method, and the differences were compared by the log-rank test. The number of Infinium assay probes showing DNA hyper- or hypomethylation in each cluster and the average DNA methylation levels ($\Delta\beta_{T-N}$) of each cluster were examined using Wilcoxon rank sum test at a significance level of $P < 0.05$. The CpG sites discriminating the clusters were identified by Fisher's exact test and random forest analysis (27).

## Results

*DNA methylation alterations during renal carcinogenesis*

First, DNA methylation levels of representative CpG sites based on the Infinium assay were clearly verified using a highly quantitative pyrosequencing method (Supplementary Figure S2, available at *Carcinogenesis* Online). With regard to the well-known methylation-silencing Von Hippel–Lindau tumor-suppressor gene (probe Target ID: cg22782492), DNA hypermethylation ($\Delta\beta_{T-N} > 0.1$) was detected in 12 (12%) of 104 patients, for whom both N and T samples were assayed in the same experimental batch. This incidence corresponded to that in previous reports (28,29). Taken together, the data confirmed the reliability of the present Infinium assay.

Although precancerous conditions in the kidney have been rarely described, our previous study suggested that N samples are already at precancerous stages, from the viewpoint of altered DNA methylation, despite the absence of any remarkable histological changes and the lack of association with chronic inflammation and persistent infection with viruses or other pathogenic microorganisms (17–20). (a) In fact, the logistic model adjusted by sex, age and experimental batch revealed that DNA methylation levels on 4830 probes were already altered in N samples compared with those in C samples (FDR, $q = 0.01$, Table I). (b) In order to reveal DNA methylation alterations inherited by clear cell RCCs themselves, ordered differences of DNA methylation level from C to N and then to T samples were examined by the cumulative logit model adjusted by sex, age and experimental batch. Ordered differences from C to N and then to T samples were observed on 11 089 probes (FDR, $q = 0.01$, Table I). (c) In order to reveal the cancer-prone DNA methylation alterations, differences in DNA methylation levels between 104 paired samples of N and T assayed in the same experimental batch were examined using the Wilcoxon matched pairs test. Significant differences between N and the corresponding clear cell RCCs themselves were observed on 10 870 probes (FDR, $q = 0.01$, Table I).

DNA hypermethylation frequently occurred at the very early stages of renal carcinogenesis [(a) in Table I], whereas DNA hypomethylation was also observed during progression to established cancers [(b) and (c) in Table I]. Eight hundred and one probes satisfied all of the above criteria (a)–(c) (Table I): DNA methylation alterations on these 801 probes (Supplementary Table S2, available at *Carcinogenesis* Online) were already evident in N samples, and were inherited by and strengthened in T samples.

**Table I.** DNA methylation alterations during renal carcinogenesis

| The number of probes showing DNA hypermethylation and DNA hypomethylation | |
|---|---|
| (a) The probes on which DNA methylation levels were altered in samples of non-cancerous renal cortex tissue (N) obtained from patients with clear cell RCCs relative to those in samples of normal renal cortex tissue (C) obtained from patients without any primary renal tumor. (Logistic model adjusted by sex, age and experimental batch; FDR, $q = 0.01$.) | |
| DNA hypermethylation ($\beta_N > \beta_C$) | 4589[a] |
| DNA hypomethylation ($\beta_N < \beta_C$) | 241[b] |
| Total | 4830 |
| (b) The probes on which DNA methylation levels showed ordered differences from C to N, and then to tumorous tissue (T) samples. (Cumulative logit model adjusted by sex, age and experimental batch; FDR, $q = 0.01$.) | |
| DNA hypermethylation ($\beta_C < \beta_N < \beta_T$, $\beta_C < \beta_N \fallingdotseq \beta_T$ or $\beta_C \fallingdotseq \beta_N < \beta_T$) | 6653 |
| DNA hypomethylation ($\beta_C > \beta_N > \beta_T$, $\beta_C > \beta_N \fallingdotseq \beta_T$ or $\beta_C \fallingdotseq \beta_N > \beta_T$) | 4436 |
| Total | 11 089 |
| (c) The probes on which DNA methylation levels differed between T and the corresponding N samples (Wilcoxon matched pairs test; FDR, $q = 0.01$) | |
| DNA hypermethylation ($\Delta\beta_{T-N} > 0$) | 5408 |
| DNA hypomethylation ($\Delta\beta_{T-N} < 0$) | 5462 |
| Total | 10 870 |

[a]Among the 4589 probes, 2675 showed DNA hypermethylation in T samples than in C samples ($\beta_T > \beta_C$; FDR, $q = 0.01$).
[b]Among the 241 probes, 126 showed DNA hypomethylation in T samples than in C samples ($\beta_T < \beta_C$; FDR, $q = 0.01$).

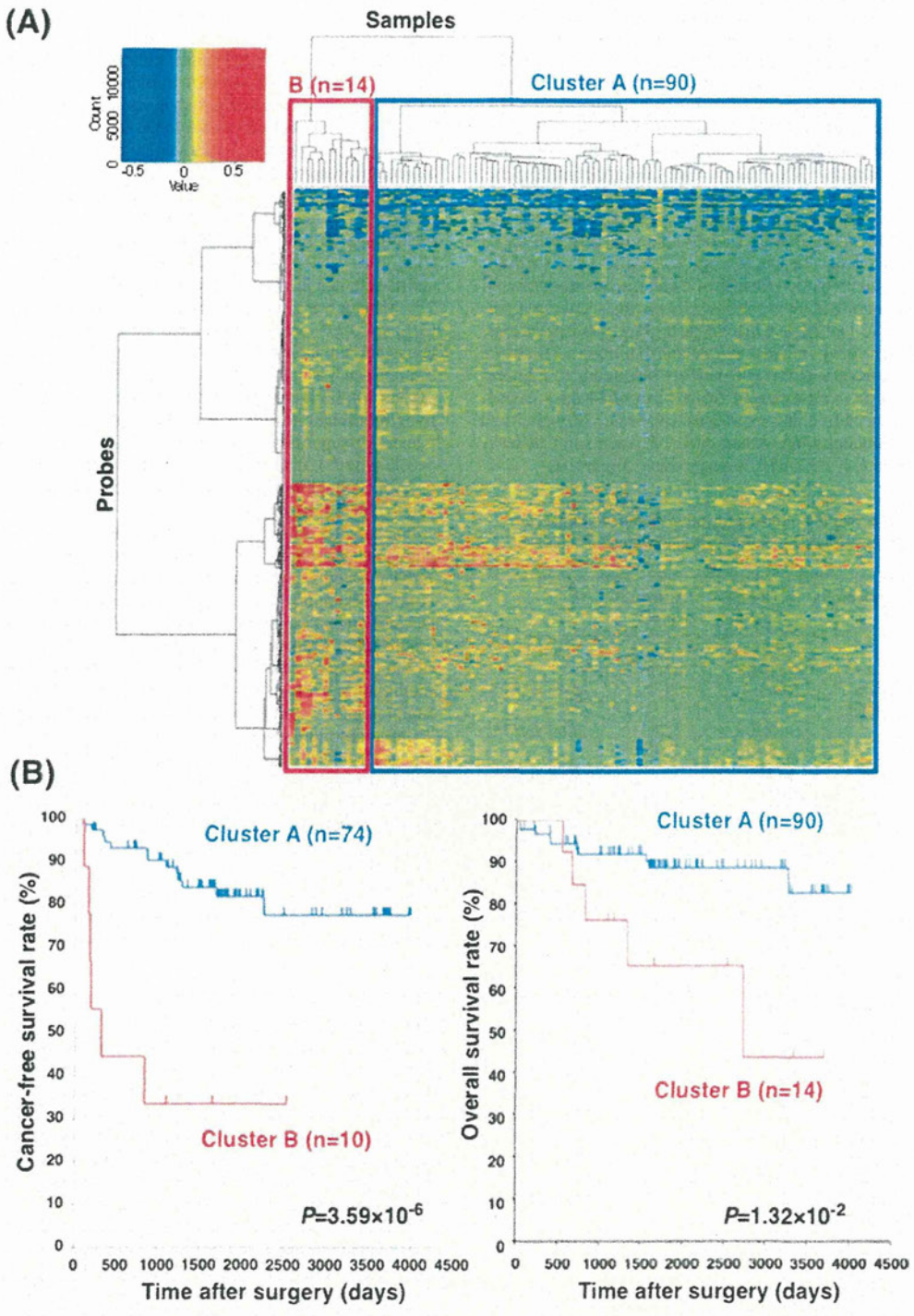


**Fig. 1.** Unsupervised hierarchical clustering using DNA methylation levels ($\Delta\beta_{T-N}$) on the 801 probes in 104 patients with clear cell RCCs. The 801 probes satisfied all of the criteria (a), (b) and (c) in 'DNA methylation alterations during renal carcinogenesis' in Results and Table I. On the 801 probes, DNA methylation alterations occurred at the precancerous stages and were inherited by and strengthened in clear cell RCCs themselves. (**A**) 104 patients with clear cell RCCs were hierarchically clustered into Cluster A ($n = 90$) and Cluster B ($n = 14$). The DNA methylation levels ($\Delta\beta_{T-N}$) are shown in the color range maps. The cluster trees for patients and probes are shown at the top and left of the panel, respectively. (**B**) The cancer-free ($P = 3.59 \times 10^{-6}$) survival rates of Stage I–III patients in Cluster B were significantly lower (log-rank test) than those of patients in Cluster A. Overall ($P = 1.32 \times 10^{-2}$) survival rates of all patients in Cluster B were significantly lower (log-rank test) than those of patients in Cluster A.

*Epigenetic clustering of clear cell RCCs*

Unsupervised hierarchical clustering using DNA methylation levels ($\Delta\beta_{T-N}$) on the above 801 probes, on which DNA methylation alterations occurred at the precancerous stages and may continuously participate in renal carcinogenesis, subclustered 104 patients with clear cell RCCs, of whom both N and T samples were assayed in the same experimental batch, into Cluster A ($n$ = 90) and Cluster B ($n$ = 14, Figure 1A). The clinicopathological parameters of clear cell RCCs belonging to Clusters A and B are summarized in Table II. (The number of samples for each TNM stage is also described in Supplementary Table S3, available at *Carcinogenesis* Online.) Epigenetic clustering of clear cell RCCs was dependent on neither age nor sex of the patients (Table II). Clear cell RCCs belonging to Cluster B had a larger diameter, more frequent macroscopically evident extranodular (type 2) or multinodular (type 3) growth, vascular involvement, renal vein tumor thrombi, infiltrating growth, tumor necrosis and renal pelvis invasion, and also had higher histological grades and pathological TNM stages than those in Cluster A (Table II). Figure 1B shows the Kaplan–Meier survival curves of patients belonging to Clusters A and B. The period covered ranged from 42 to 4024 days (mean, 1821 days). The cancer-free and overall survival rates of patients in Cluster B were significantly lower than those of patients in Cluster A ($P = 3.59 \times 10^{-6}$ and $P = 1.32 \times 10^{-2}$, respectively, Figure 1B).

**Table II.** Correlation between the subclassification of patients with clear cell RRCs based on DNA methylation profiles and the clinicopathological parameters

| Clinicopathological parameters | | Cluster A ($n$ = 90) | Cluster B ($n$ = 14) | $P$ [a] |
|---|---|---|---|---|
| Age | | 62.08 ± 10.08 | 67.36 ± 11.06 | $8.36 \times 10^{-2}$ [b] |
| Sex | Male | 63 | 11 | $5.47 \times 10^{-1}$ [c] |
| | Female | 27 | 3 | |
| Tumor diameter (cm) | | 5.10 ± 3.19 | 8.75 ± 2.85 | *$1.07 \times 10^{-4}$* [b] |
| Macroscopic configuration | Type 1 | 37 | 1 | *$6.29 \times 10^{-4}$* [c] |
| | Type 2 | 29 | 2 | |
| | Type 3 | 24 | 11 | |
| Predominant histological grades[d] | G1 | 47 | 1 | *$8.33 \times 10^{-6}$* [c] |
| | G2 | 35 | 4 | |
| | G3 | 7 | 7 | |
| | G4 | 1 | 2 | |
| Highest histological grades[e] | G1 | 8 | 0 | *$5.67 \times 10^{-4}$* [c] |
| | G2 | 43 | 1 | |
| | G3 | 24 | 4 | |
| | G4 | 15 | 9 | |
| Vascular involvement | Negative | 54 | 1 | *$2.45 \times 10^{-4}$* [c] |
| | Positive | 36 | 13 | |
| Renal vein tumor thrombi | Negative | 69 | 5 | *$3.38 \times 10^{-3}$* [c] |
| | Positive | 21 | 9 | |
| Predominant growth pattern[d] | Expansive | 84 | 7 | *$1.86 \times 10^{-4}$* [c] |
| | Infiltrative | 6 | 7 | |
| Most aggressive growth pattern[e] | Expansive | 57 | 4 | *$2.06 \times 10^{-3}$* [c] |
| | Infiltrative | 33 | 10 | |
| Tumor necrosis | Negative | 71 | 2 | *$4.86 \times 10^{-6}$* [c] |
| | Positive | 19 | 12 | |
| Invasion to renal pelvis | Negative | 83 | 10 | *$3.98 \times 10^{-2}$* [c] |
| | Positive | 7 | 4 | |
| Pathological TNM stage | Stage I | 50 | 0 | *$5.41 \times 10^{-5}$* [c] |
| | Stage II | 1 | 1 | |
| | Stage III | 23 | 9 | |
| | Stage IV | 16 | 4 | |

The number of samples in each TNM stage was described in Supplementary Table S3, available at *Carcinogenesis* Online.

[a]*P*-values of <0.05 are in italics.

[b]Wilcoxon rank sum test.

[c]Fisher's exact test.

[d]If the tumor showed heterogeneity, findings in the predominant area were described.

[e]If the tumor showed heterogeneity, the most aggressive features of the tumor were described.

*DNA methylation profiles of clear cell RCCs belonging to each cluster*

The distribution of DNA methylation levels ($\Delta\beta_{T-N}$) in all 26 454 probes for 104 clear cell RCCs belonging to Cluster A or B is summarized along chromosomes in Figure 2A. Clear cell RCCs belonging to Cluster B clearly showed accumulation of DNA hypermethylation ($\Delta\beta_{T-N} > 0.1$) relative to DNA hypomethylation, whereas clear cell RCCs belonging to Cluster A showed greater DNA hypomethylation ($\Delta\beta_{T-N} < -0.1$) relative to DNA hypermethylation (Figure 2A).

The proportions of the probes showing the various degrees of DNA hypermethylation in T samples compared with the corresponding N samples ($\Delta\beta_{T-N} > 0.1$, 0.2, 0.3, 0.4 or 0.5) for all 26 454 probes, and the proportions of the probes showing various degrees of DNA hypomethylation in T samples compared with the corresponding N samples ($\Delta\beta_{T-N} < -0.1$, −0.2, −0.3, −0.4 or −0.5) for all 26 454 probes in clear cell RCCs belonging to Clusters A and B are summarized in Figure 2B. Although the probes showing prominent DNA hypomethylation ($\Delta\beta_{T-N} < -0.5$) were accumulated slightly more in Cluster B than in Cluster A, the incidence of DNA hypomethylation in Clusters A and B did not reach a statistically significant difference ($\Delta\beta_{T-N} < -0.1$, −0.2, −0.3 or −0.4, Figure 2B). On the other hand, the probes showing DNA hypermethylation were markedly accumulated in Cluster B relative to Cluster A, regardless of the degree of DNA hypermethylation ($\Delta\beta_{T-N} > 0.1$, 0.2, 0.3, 0.4 or 0.5, Figure 2B). These data indicate that clear cell RCCs belonging to Cluster B are characterized by accumulation of DNA hypermethylation.

The top 61 probes (including the 60th and 61st, which showed equivalent $P$-values) on which DNA methylation levels ($\Delta\beta_{T-N}$) differed markedly between Clusters A and B ($P < 1.056 \times 10^{-6}$, Wilcoxon rank sum test) are listed in Supplementary Table S4, available at *Carcinogenesis* Online. Although only 19 246 probes (72.8%) out of the total of 26 454 were located within CpG islands, 60 (98.4%) of the top 61 probes located within CpG islands showed DNA hypermethylation in clear cell RCCs belonging to Cluster B ($\Delta\beta_{T-N} > 0.097$, Supplementary Table S4, available at *Carcinogenesis* Online): only 1 probe among the top 61 was located within a non-CpG island and showed DNA hypomethylation ($\Delta\beta_{T-N} = -0.425 \pm 0.096$ in Cluster B). Taken together, the data indicated that Cluster B is significantly correlated with clinicopathological phenotype and characterized by frequent DNA hypermethylation on CpG islands. Such characteristics of clear cell RCCs in Cluster B are similar to those of CpG island methylator phenotype (CIMP)-positive cancers (30,31) in other well-studied organs, such as those of the colon (32) and stomach (33). In other words, our single-CpG-resolution methylome analysis identified, for the first time, CIMP-positive clear cell RCCs as Cluster B.

*Hallmark CpG sites of CIMP-positive clear cell RCCs*

Scattergrams of DNA methylation levels ($\beta$ values) in T and the corresponding N samples from representative patients with clear cell RCCs belonging to Clusters A and B (Supplementary Figure S3, available at *Carcinogenesis* Online) indicated that probes for which DNA methylation levels were low in the N samples and for which the degree of DNA hypermethylation in T samples relative to the corresponding N samples was prominent (marked by red circles in panels E to H in Supplementary Figure S3, available at *Carcinogenesis* Online) were obvious only in Cluster B, and not in Cluster A.

Therefore, in order to discriminate clear cell RCCs belonging to Cluster B from those belonging to Cluster A, we first focused on the probes for which the average $\beta$ value in all N samples was less than 0.2 and the incidence of more than $0.4\Delta\beta_{T-N}$ was markedly higher in Cluster B relative to Cluster A ($P < 1.98 \times 10^{-6}$, Fisher's exact test). Among such probes, 16 (the FAM150A, GRM6, ZNF540, ZFP42, ZNF154, RIMS4, PCDHAC1, KHDRBS2, ASCL2, KCNQ1, PRAC, ZNF154, WNT3A, TRH, FAM78A and ZNF671 genes) showed $>0.4\Delta\beta_{T-N}$ in 6 (42.8%) or more RCCs among the 14 belonging to Cluster B, but only in 2 (2.2%) or fewer RCCs among the 90 belonging to Cluster A (Table IIIA). DNA methylation levels ($\Delta\beta_{T-N}$) on the 16 CpG sites differed completely between Clusters A and B (Supplementary Figure S4, available at *Carcinogenesis* Online). In addition,

random forest analysis (27) (Supplementary Figure S5, available at *Carcinogenesis* Online) using the 869 probes on which DNA methylation levels ($\Delta\beta_{T-N}$) differed significantly between Clusters A and B [FDR ($q$ = 0.01)] identified the top four probes that were able to discriminate Cluster B from Cluster A in Table IIIB. Two probes were shared by Tables IIIA and IIIB. Thus, CpG sites on the 18 probes can be considered as hallmarks of CIMP-positive clear cell RCCs, i.e. clear cell RCCs belonging to Cluster B.

## Discussion

Here, we have reported the results of methylome analysis of 245 renal tissue samples at single-CpG resolution. To our knowledge, no study involving Infinium analysis of such a large number of renal tissue samples has been reported to date. We have been focusing on DNA methylation alterations at the precancerous stage: our previous studies using methylation-specific PCR, combined bisulfite restriction enzyme analysis and bacterial artificial chromosome arrays suggested that N samples are already at the precancerous stage associated with DNA methylation alterations (17–20). First, we identified the probes on which DNA methylation status in N samples were significantly altered relative to those in C samples. The single-CpG-resolution analysis revealed that the DNA methylation status of 4830 CpG sites was actually altered at the precancerous stage in comparison to normal renal cortex tissue samples. In addition, it was revealed that alterations at the precancerous stages tended to involve DNA hypermethylation [Table I(a)]. Among the 801 probes we selected, DNA methylation alterations occurred at the precancerous stage and were inherited by, and strengthened in, clear cell RCCs themselves, indicating that DNA methylation alterations on the 801 probes may participate continuously in renal carcinogenesis from the precancerous stage until cancers have become established. The DNA methylation profiles of these 801 probes clustered clear cell RCCs into clinicopathologically valid subclusters: clear cell RCCs belonging to Cluster B showed clinicopathological parameters reflecting tumor aggressiveness, and patients with Cluster B tumors showed a poorer outcome. Quantitative reverse transcription–PCR analysis indicated that DNA hypermethylation may result in significantly reduced expression of representative genes listed in Tables IIIA and IIIB and Supplementary Table S4, available at *Carcinogenesis* Online (Supplementary Table S5, available at *Carcinogenesis* Online). These findings suggest that DNA

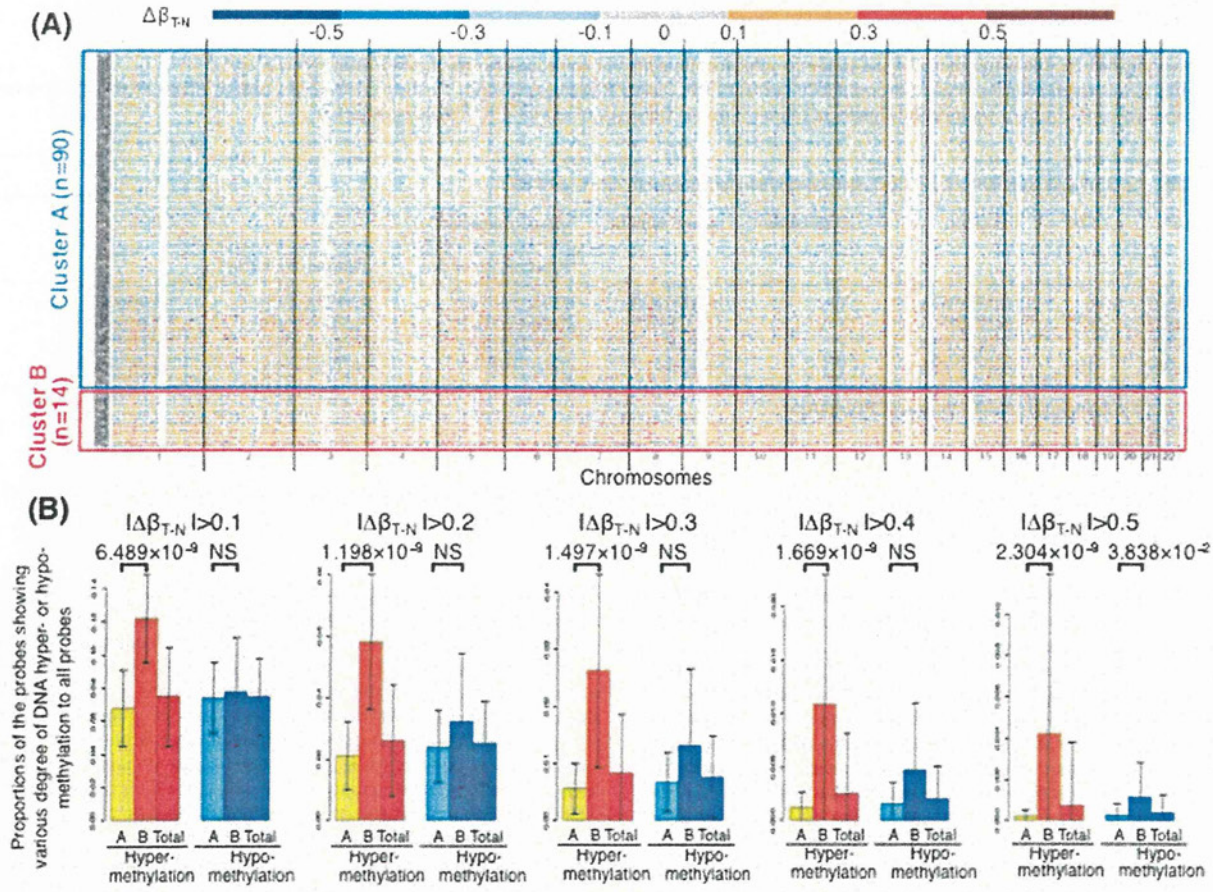


**Fig. 2.** (**A**) Distribution of DNA methylation levels ($\Delta\beta_{T-N}$) in all 26 454 probes in 104 clear cell RCCs belonging to Cluster A or B. The DNA methylation levels are shown in the color range maps. Clear cell RCCs belonging to Cluster A are skewed toward DNA hypomethylation ($\Delta\beta_{T-N} < -0.1$, cold color) relative to DNA hypermethylation (warm color). Clear cell RCCs belonging to Cluster B clearly showed accumulation of DNA hypermethylation ($\Delta\beta_{T-N} > 0.1$, warm color) relative to DNA hypomethylation (cold color). (**B**) The proportions of the probes showing the various degrees of DNA hypermethylation, when the tumor tissue (T) sample was compared with the corresponding non-cancerous renal cortex tissue (N) sample ($\Delta\beta_{T-N} > 0.1$, 0.2, 0.3, 0.4 or 0.5, warm color), to all probes, and the proportions of the probes showing the various degrees of DNA hypomethylation, when the T sample was compared with the corresponding N sample ($\Delta\beta_{T-N} < -0.1$, −0.2, −0.3, −0.4 or −0.5, cold color), to all probes in Clusters A and B. Bar, standard deviation. The probes showing DNA hypermethylation were markedly accumulated in Cluster B relative to Cluster A, regardless of the degree of DNA hypermethylation ($\Delta\beta_{T-N} > 0.1$, 0.2, 0.3, 0.4 or 0.5). The probes showing prominent DNA hypomethylation ($\Delta\beta_{T-N} < -0.5$) were slightly accumulated in Cluster B compared with Cluster A. These data indicated that clear cell RCCs belonging to Cluster B are mainly characterized by accumulation of DNA hypermethylation.

**Table IIIA.** CpG sites as hallmarks of the CpG island methylator phenotype of clear cell RRCs

| Target ID[a] | Chr[b] | Position[c] | CpG island[d] | Gene symbol | The number of tumors whose $\Delta\beta_{T-N} > 0.4$ (%)[e] | | $P$[f] |
|---|---|---|---|---|---|---|---|
| | | | | | Cluster A ($n = 90$) | Cluster B ($n = 14$) | |
| cg17162024 | 8 | 53,478,454 | Y | FAM150A | 2 (2.2) | 12 (85.7) | $4.60 \times 10^{-12}$ |
| cg14859460 | 5 | 178,422,244 | Y | GRM6 | 0 (0) | 10 (71.4) | $3.84 \times 10^{-11}$ |
| cg03975694 | 19 | 38,042,472 | Y | ZNF540 | 2 (2.2) | 9 (64.3) | $3.64 \times 10^{-8}$ |
| cg06274159 | 4 | 188,916,867 | Y | ZFP42 | 1 (1.1) | 8 (57.1) | $9.91 \times 10^{-8}$ |
| cg08668790 | 19 | 58,220,662 | Y | ZNF154 | 1 (1.1) | 8 (57.1) | $9.91 \times 10^{-8}$ |
| cg19332710 | 20 | 43,438,865 | Y | RIMS4 | 2 (2.2) | 8 (57.1) | $4.68 \times 10^{-7}$ |
| cg12629325 | 5 | 140,306,458 | Y | PCDHAC1 | 2 (2.2) | 7 (50) | $5.10 \times 10^{-6}$ |
| cg18239753 | 6 | 62,995,963 | Y | KHDRBS2 | 2 (2.2) | 7 (50) | $5.10 \times 10^{-6}$ |
| cg06263495 | 11 | 2,292,004 | Y | ASCL2 | 2 (2.2) | 7 (50) | $5.10 \times 10^{-6}$ |
| cg17575811 | 11 | 2,466,409 | Y | KCNQ1 | 1 (1.1) | 7 (50) | $1.21 \times 10^{-6}$ |
| cg12374721 | 17 | 46,799,640 | Y | PRAC | 2 (2.2) | 7 (50) | $5.10 \times 10^{-6}$ |
| cg21790626 | 19 | 58,220,494 | Y | ZNF154 | 0 (0) | 7 (50) | $1.62 \times 10^{-7}$ |
| cg01322134 | 1 | 228,194,448 | Y | WNT3A | 0 (0) | 6 (42.9) | $1.98 \times 10^{-6}$ |
| cg01009664 | 3 | 129,693,613 | Y | TRH | 0 (0) | 6 (42.9) | $1.98 \times 10^{-6}$ |
| cg12998491 | 9 | 134,152,531 | Y | FAM78A | 0 (0) | 6 (42.9) | $1.98 \times 10^{-6}$ |
| cg19246110 | 19 | 58,238,928 | Y | ZNF671 | 0 (0) | 6 (42.9) | $1.98 \times 10^{-6}$ |

[a]Probe ID for the Infinium HumanMethylation27 Bead Array.
[b]Chromosome.
[c]National Center for Biotechnology Information (NCBI) Database (Genome Build 37).
[d]Y means CpG island.
The probes satisfied the following criteria: (i) the average $\beta$ value for all samples of non-cancerous renal cortex tissue (N) was <0.2, (ii) $>0.4\Delta\beta_{T-N}$ was observed in six or more clear cell RCCs (≥42.9%)[e] in Cluster B, whereas $>0.4\Delta\beta_{T-N}$ in two or fewer clear cell RCCs (≤2.2%)[e] in Cluster A and (iii) the incidence of $>0.4\Delta\beta_{T-N}$ was markedly higher in Cluster B than in Cluster A ($P < 1.98 \times 10^{-6}$, Fisher's exact test[f]).

**Table IIIB.** CpG sites as hallmarks of the CpG island methylator phenotype of clear cell RRCs

| Target ID[a] | Chr[b] | Position[c] | CpG island[d] | Gene symbol | $\Delta\beta_{T-N}$ (mean ± SD) | | $P$[e] |
|---|---|---|---|---|---|---|---|
| | | | | | Cluster A ($n = 90$) | Cluster B ($n = 14$) | |
| cg17162024 | 8 | 53,478,454 | Y | FAM150A[f] | 0.126±0.120 | 0.499±0.184 | $3.40 \times 10^{-7}$ |
| cg22040627 | 17 | 6,617,030 | Y | SLC13A5 | 0.045±0.072 | 0.283±0.103 | $2.64 \times 10^{-7}$ |
| cg14859460 | 5 | 178,422,244 | Y | GRM6[f] | 0.077±0.105 | 0.434±0.184 | $1.10 \times 10^{-7}$ |
| cg09260089 | 10 | 134,599,860 | Y | NKX6-2 | 0.078±0.083 | 0.372±0.150 | $2.26 \times 10^{-7}$ |

[a]Probe ID of the Infinium HumanMethylation27 Bead Array.
[b]Chromosome.
[c]NCBI Database (Genome Build 37).
[d]Y means CpG island.
[e]Top four probes capable of discriminating Cluster B from Cluster A identified by random forest analysis (Supplementary Figure S5, available at *Carcinogenesis* Online) using the 869 probes on which the DNA methylation levels ($\Delta\beta_{T-N}$) were differed significantly between Clusters A and B (Wilcoxon rank sum test).
[f]The FAM150A and GRM6 genes were shared by Tables IIIA and IIIB.

methylation alterations occurring at the precancerous stage determine both the aggressiveness of RCCs and the outcome of affected patients through alterations of gene expression levels.

Unsupervised hierarchical clustering based on our previous study using bacterial artificial chromosome arrays also clustered clear cell RCCs into clinicopathologically valid subclusters: 14% of examined RCCs belonged to a subcluster showing clinicopathological parameters reflecting tumor aggressiveness and poorer patient outcome (19). DNA methylation profiles in N samples based on BAMCA data were also inherited by the corresponding clear cell RCC developing in the same patient. In this study, 14% of the clear cell RCCs subjected to Infinium analysis belonged to Cluster B. BAMCA is suitable for detecting DNA methylation alterations occurring in a coordinated manner on individual large regions of chromosomes (34–37), whereas 27 000 Infinium array is suitable for detecting DNA methylation alterations on promoter regions of specific genes. Different methodologies identified similar clinicopathologically valid subclusters of RCCs, indicating that such clustering based on DNA methylation profiles is not accidental but reproducible, and may reflect the distinct epigenetic pathway of renal carcinogenesis.

In contrast to Cluster A, which appeared to be characterized by accumulation of DNA hypomethylation (Figure 2A), Cluster B was clearly characterized by accumulations of DNA hypermethylation on CpG islands. Since Cluster B was significantly associated with both frequent DNA hypermethylation on CpG islands and distinct clinicopathological phenotypes of clear cell RCCs, RCCs belonging to Cluster B can be recognized as CIMP-positive clear cell RCCs on the basis of the definition of well-studied CIMP-positive cancers (30,31) such as colorectal cancer (32) and stomach cancer (33), although Morris *et al.* (28) previously considered that the relevance of the CIMP-positive phenotype to RCCs had not yet been clearly defined. Although McRonald *et al.* (29) suggested that a subset of RCCs might display CIMP based on findings indicating that the distribution of the number of methylated CpGs in individual tumors differed from the expected Poisson distribution, they did not identify distinct CpG sites that could become hallmarks for CIMP in the kidney. It has been suggested that, in order to identify CIMP-positive cancers in specific organs, marker CpG sites or genes that are specific to each organ or histological type of tumor should be used (38), rather than classical CIMP marker genes (30,31) that were originally identified in colorectal cancers. The present single-CpG-resolution analysis identified such hallmark CpG sites for the first time. Using the 18 CpG sites in Tables IIIA and IIIB, CIMP-positive RCCs or RCCs equivalent to those in the present Cluster B could be reproducibly identified. These 18 CpG sites may be useful for further clarifying the molecular basis of the epigenetic pathway of renal carcinogenesis.

DNA methylation alterations are known to result in chromosomal instability through chromatin configuration changes (39). In fact, germline mutations of the de novo DNA methyltransferase DNMT3B gene have been reported in patients with immunodeficiency, centromeric instability and facial anomalies (ICF) syndrome, a rare recessive autosomal disorder characterized by DNA hypomethylation of pericentromeric satellite regions (40). In HCCs and urothelial carcinomas, DNA hypomethylation of these regions is correlated with copy number alterations on chromosomes 1 (41) and 9 (42), respectively, where satellite regions are plentiful. Correlations between the clustering based on Infinium assay and copy number alterations should be further examined.

Taken together, the data suggest that in CIMP-positive clear cell RCCs belonging to Cluster B, DNA hypermethylation of distinct CpG islands participates even in the very early and precancerous stages. Such DNA methylation alterations occurring in the precancerous stages may induce more aggressive tumor phenotypes and poorer patient outcome in Cluster B. On the other hand, in the other pathway of renal carcinogenesis leading to clear cell RCCs in Cluster A, DNA hypomethylation may be a later event (Table I) than DNA hypermethylation on CpG islands. We are now performing exome, transcriptome and proteome analyses of RCCs belonging to both clusters. Such multilayer omics analyses may identify the upstream genetic events inducing DNA methylation profiles and key signal pathways that characterize Clusters A and B.

## Supplementary material

Supplementary Figures S1–S5 and Tables S1–S5 can be found at http://carcin.oxfordjournals.org/.

## Funding

Program for Promotion of Fundamental Studies in Health Sciences of the National Institute of Biomedical Innovation (NiBio); Grant-in-Aid for the Third Term Comprehensive 10-Year Strategy for Cancer Control from the Ministry of Health, Labor and Welfare of Japan; National Cancer Center Research and Development Fund; Grants-in-Aid for Scientific Research (B) and for Young Scientists (B) from the Japan Society for the Promotion of Science (JSPS).

## Acknowledgements

*Conflict of Interest Statement:* None declared.

## References

1. Ljungberg,B. *et al.* (2011) The epidemiology of renal cell carcinoma. *Eur. Urol.*, **60**, 615–621.
2. Arai,E. *et al.* (2011) Genetic and epigenetic alterations during renal carcinogenesis. *Int. J. Clin. Exp. Pathol.*, **4**, 58–73.
3. Baldewijns,M.M. *et al.* (2010) VHL and HIF signalling in renal cell carcinogenesis. *J. Pathol.*, **221**, 125–138.
4. Barrett,I.P. (2010) Cancer genome analysis informatics. *Methods Mol. Biol.*, **628**, 75–102.
5. Zhang,J. *et al.* (2011) International Cancer Genome Consortium Data Portal--a one-stop shop for cancer genomics data. *Database (Oxford)*, **2011**, bar026.
6. Brannon,A.R. *et al.* (2010) Renal cell carcinoma: where will the state-of-the-art lead us? *Curr. Oncol. Rep.*, **12**, 193–201.
7. Dalgliesh,G.L. *et al.* (2010) Systematic sequencing of renal carcinoma reveals inactivation of histone modifying genes. *Nature*, **463**, 360–363.
8. van Haaften,G. *et al.* (2009) Somatic mutations of the histone H3K27 demethylase gene UTX in human cancer. *Nat. Genet.*, **41**, 521–523.
9. Varela,I. *et al.* (2011) Exome sequencing identifies frequent mutation of the SWI/SNF complex gene PBRM1 in renal carcinoma. *Nature*, **469**, 539–542.
10. Baylin,S.B. *et al.* (2011) A decade of exploring the cancer epigenome - biological and translational implications. *Nat. Rev. Cancer*, **11**, 726–734.
11. Boumber,Y. *et al.* (2011) Epigenetics in cancer: what's the future? *Oncology (Williston Park)*, **25**, 220–226, 228.
12. Jones,P.A. *et al.* (2007) The epigenomics of cancer. *Cell*, **128**, 683–692.
13. Kanai,Y. (2010) Genome-wide DNA methylation profiles in precancerous conditions and cancers. *Cancer Sci.*, **101**, 36–45.
14. Arai,E. *et al.* (2010) DNA methylation profiles in precancerous tissue and cancers: carcinogenetic risk estimation and prognostication based on DNA methylation status. *Epigenomics*, **2**, 467–481.
15. Kanai,Y. (2008) Alterations of DNA methylation and clinicopathological diversity of human cancers. *Pathol. Int.*, **58**, 544–558.
16. Kanai,Y. *et al.* (2007) Alterations of DNA methylation associated with abnormalities of DNA methyltransferases in human cancers during transition from a precancerous to a malignant state. *Carcinogenesis*, **28**, 2434–2442.
17. Arai,E. *et al.* (2008) Genetic clustering of clear cell renal cell carcinoma based on array-comparative genomic hybridization: its association with DNA methylation alteration and patient outcome. *Clin. Cancer Res.*, **14**, 5531–5539.
18. Arai,E. *et al.* (2006) Regional DNA hypermethylation and DNA methyltransferase (DNMT) 1 protein overexpression in both renal tumors and corresponding nontumorous renal tissues. *Int. J. Cancer*, **119**, 288–296.
19. Arai,E. *et al.* (2009) Genome-wide DNA methylation profiles in both precancerous conditions and clear cell renal cell carcinomas are correlated with malignant potential and patient outcome. *Carcinogenesis*, **30**, 214–221.
20. Arai,E. *et al.* (2011) Genome-wide DNA methylation profiles in renal tumors of various histological subtypes and non-tumorous renal tissues. *Pathobiology*, **78**, 1–9.
21. Bibikova,M. *et al.* (2009) Genome-wide DNA methylation profiling using Infinium® assay. *Epigenomics*, **1**, 177–200.
22. Eble,J.N. *et al.* (2004) Renal cell carcinoma. *World Health Organization Classification of Tumours. Pathology and Genetics. Tumours of the Urinary System and Male Genital Organs*. IARC Press, Lyon, pp. 10–43.
23. Fuhrman,S.A. *et al.* (1982) Prognostic significance of morphologic parameters in renal cell carcinoma. *Am. J. Surg. Pathol.*, **6**, 655–663.
24. Sobin,L.H. *et al.* (2002) International Union Against Cancer (UICC). *TNM Classification of Malignant Tumors*. 6th edn. Wiley-Liss, New York, pp. 193–195.
25. Kanai,T. *et al.* (1987) Pathology of small hepatocellular carcinoma. A proposal for a new gross classification. *Cancer*, **60**, 810–819.
26. Sambrook,J. *et al.* (2001) *Molecular Cloning: A Laboratory Manual*. 3rd edn. Cold Spring Harbor Laboratory Press, Cold Spring Harbor, NY, pp. 6.14–6.15.
27. Breiman,L. (2001) Random forests. *Mach. Learn.*, **45**, 5–32.
28. Morris,M.R. *et al.* (2010) Epigenetics of renal cell carcinoma: the path towards new diagnostics and therapeutics. *Genome Med.*, **2**, 59.
29. McRonald,F.E. *et al.* (2009) CpG methylation profiling in VHL related and VHL unrelated renal cell carcinoma. *Mol. Cancer*, **8**, 31.
30. Issa,J.P. (2004) CpG island methylator phenotype in cancer. *Nat. Rev. Cancer*, **4**, 988–993.
31. Toyota,M. *et al.* (1999) CpG island methylator phenotype in colorectal cancer. *Proc. Natl. Acad. Sci. U.S.A.*, **96**, 8681–8686.
32. Shen,L., *et al.* (2007) Integrated genetic and epigenetic analysis identifies three different subclasses of colon cancer. *Proc. Natl. Acad. Sci. U.S.A.*, **104**, 18654–18659.
33. Toyota,M. *et al.* (1999) Aberrant methylation in gastric cancer associated with the CpG island methylator phenotype. *Cancer Res.*, **59**, 5438–5442.
34. Nagashio,R. *et al.* (2011) Carcinogenetic risk estimation based on quantification of DNA methylation levels in liver tissue at the precancerous stage. *Int. J. Cancer*, **129**, 1170–1179.
35. Gotoh,M. *et al.* (2011) Diagnosis and prognostication of ductal adenocarcinomas of the pancreas based on genome-wide DNA methylation profiling by bacterial artificial chromosome array-based methylated CpG island amplification. *J. Biomed. Biotechnol.*, **2011**, 780–836.
36. Nishiyama,N. *et al.* (2010) Genome-wide DNA methylation profiles in urothelial carcinomas and urothelia at the precancerous stage. *Cancer Sci.*, **101**, 231–240.
37. Arai,E. *et al.* (2009) Genome-wide DNA methylation profiles in liver tissue at the precancerous stage and in hepatocellular carcinoma. *Int. J. Cancer*, **125**, 2854–2862.
38. Abe,M. *et al.* (2008) Identification of genes targeted by CpG island methylator phenotype in neuroblastomas, and their possible integrative involvement in poor prognosis. *Oncology*, **74**, 50–60.
39. Eden,A. *et al.* (2003) Chromosomal instability and tumors promoted by DNA hypomethylation. *Science*, **300**, 455.
40. Hansen,R.S. *et al.* (1999) The DNMT3B DNA methyltransferase gene is mutated in the ICF immunodeficiency syndrome. *Proc. Natl. Acad. Sci. U.S.A.*, **96**, 14412–14417.
41. Wong,N. *et al.* (2001) Hypomethylation of chromosome 1 heterochromatin DNA correlates with q-arm copy gain in human hepatocellular carcinoma. *Am. J. Pathol.* **59**, 465–471.
42. Nakagawa,T. *et al.* (2005) DNA hypomethylation on pericentromeric satellite regions significantly correlates with loss of heterozygosity on chromosome 9 in urothelial carcinomas. *J. Urol.*, **173**, 243–246.

*Received December 11, 2012; revised April 17, 2012; accepted May 11, 2012*

EUROPEAN UROLOGY 63 (2013) 1091–1100

available at www.sciencedirect.com
journal homepage: www.europeanurology.com

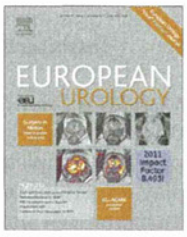

European Association of Urology

Urothelial Cancer

# Methylation of a Panel of MicroRNA Genes Is a Novel Biomarker for Detection of Bladder Cancer

*Takashi Shimizu*[a,b], *Hiromu Suzuki*[b,c,*], *Masanori Nojima*[c,d], *Hiroshi Kitamura*[a], *Eiichiro Yamamoto*[b,c], *Reo Maruyama*[b,c], *Masami Ashida*[b], *Tomo Hatahira*[b], *Masahiro Kai*[b], *Naoya Masumori*[a], *Takashi Tokino*[e], *Kohzoh Imai*[f], *Taiji Tsukamoto*[a,**], *Minoru Toyota*[b]

[a] *Department of Urology, Sapporo Medical University, Sapporo, Japan;* [b] *Department of Molecular Biology, Sapporo Medical University, Sapporo, Japan;* [c] *First Department of Internal Medicine, Sapporo Medical University, Sapporo, Japan;* [d] *Department of Public Health, Sapporo Medical University, Sapporo, Japan;* [e] *Medical Genome Science, Research Institute for Frontier Medicine, Sapporo Medical University, Sapporo, Japan;* [f] *Division of Novel Therapy for Cancer, The Advanced Clinical Research Center, The Institute of Medical Science, The University of Tokyo, Tokyo, Japan*

**Article info**

*Article history:*
Accepted November 13, 2012
**Published online ahead of print on November 23, 2012**

*Keywords:*
Biomarker
Bladder cancer
DNA methylation
MicroRNA
Urinary test

**Abstract**

***Background:*** Dysregulation of microRNAs (miRNAs) has been implicated in bladder cancer (BCa), although the mechanism is not fully understood.
***Objective:*** We aimed to explore the involvement of epigenetic alteration of miRNA expression in BCa.
***Design, setting, and participants:*** Two BCa cell lines (T24 and UM-UC-3) were treated with 5-aza-2′-deoxycytidine (5-aza-dC) and 4-phenylbutyric acid (PBA), after which their miRNA expression profiles were analyzed using a TaqMan array (Life Technologies, Carlsbad, CA, USA). Bisulfite pyrosequencing was used to assess miRNA gene methylation in 5 cancer cell lines, 83 primary tumors, and 120 preoperative and 47 postoperative urine samples.
***Outcome measurements and statistical analysis:*** Receiver operating characteristic (ROC) curve analysis was used to assess the diagnostic performance of the miRNA gene panel.
***Results and limitations:*** Of 664 miRNAs examined, 146 were upregulated by 5-aza-dC plus PBA. CpG islands were identified in the proximal upstream of 23 miRNA genes, and 12 of those were hypermethylated in cell lines. Among them, miR-137, miR-124-2, miR-124-3, and miR-9-3 were frequently and tumor-specifically methylated in primary cancers (miR-137: 68.7%; miR-124-2: 50.6%; miR-124-3: 65.1%; miR-9-3: 45.8%). Methylation of the same four miRNAs in urine specimens enabled BCa detection with 81% sensitivity and 89% specificity; the area under the ROC curve was 0.916. Ectopic expression of silenced miRNAs in BCa cells suppressed growth and cell invasion.
***Conclusions:*** Our results indicate that epigenetic silencing of miRNA genes may be involved in the development of BCa and that methylation of miRNA genes could be a useful biomarker for cancer detection.


* Corresponding author. Department of Molecular Biology, Sapporo Medical University, S1, W17, Chuo-Ku, Sapporo 060-8556, Japan. Tel. +81 11 611 2111; Fax: +81 11 622 1918.
** Corresponding author. Department of Urology, Sapporo Medical University, S1, W16, Chuo-Ku, Sapporo 060-8543, Japan. Tel. +81 11 611 2111; Fax: +81 11 612 2709.
E-mail addresses: hsuzuki@sapmed.ac.jp (H. Suzuki), taijit@sapmed.ac.jp (T. Tsukamoto).

0302-2838/$ – see back matter 
http://dx.doi.org/10.1016/j.eururo.2012.11.030

## 1. Introduction

*MicroRNAs* (miRNAs) are a group of small noncoding RNAs that negatively regulate the translation and stability of partially complementary target mRNAs. In that way, they play important roles in a wide array of biologic processes, including cell proliferation, differentiation, and apoptosis [1]. Increasing evidence suggests that dysregulation of miRNA expression contributes to the initiation and progression of human cancer [2,3]. Altered miRNA expression is thought to play an important role in the pathogenesis of bladder cancer (BCa) and in certain tumor phenotypes. For instance, high-grade BCa exhibits upregulation of several miRNAs, including miR-21, which suppresses p53 function [4]. In addition, miR-21-to-miR-205 expression ratios are elevated in invasive BCa cells [5], while miR-200 family members regulate epithelial-to-mesenchymal transition by targeting transcription repressors ZEB1 and ZEB2 in BCa cells [6].

Although the mechanisms underlying miRNA dysregulation in cancer are not yet fully understood, recent studies have shown that the silencing of several miRNAs is tightly linked to epigenetic mechanisms, including histone modification and DNA methylation [7,8]. For example, treatment with a histone deacetylase (HDAC) inhibitor and a DNA methyltransferase (DNMT) inhibitor restored expression of various miRNAs in cancer cells [7,9], and the list of miRNA genes methylated in cancer is rapidly growing [10]. Studies have also shown that restoration of epigenetically silenced miRNAs may be an effective strategy for treating cancer and that aberrant methylation of miRNA genes could be a useful biomarker for cancer detection [10,11]. In addition, it was recently shown that the silencing of miRNA expression in BCa is associated with DNA methylation, often involving the CpG island (CGI) or CpG shore [12,13]. In an effort to identify novel biomarkers and treatment targets in BCa, we aimed to identify miRNAs epigenetically silenced in BCa cells by screening for miRNAs whose expression is upregulated by DNA demethylation and HDAC inhibition. We also investigated the methylation of miRNA genes in urine specimens and assessed its clinical usefulness as a biomarker for detection of BCa.

## 2. Materials and methods

### 2.1. Cell lines and tissue samples

BCa cell lines (T24, UM-UC-3, HT-1197, HT-1376, SW780, and 5637) and a normal urothelial cell line (SV-HUC-1) were obtained from the American Type Culture Collection (ATCC, Manassas, VA, USA; Supplementary Table 1). A colorectal cancer cell line HCT116 harboring genetic disruptions within the DNMT1 and DNMT3B loci (DNMTs KO) have been described previously [8]. T24 and UM-UC-3 cells were treated first with 1 μM or 0.1 μM 5-aza-2′-deoxycytidine (5-aza-dC; Sigma-Aldrich, St Louis, MO, USA) for 72 h, and then with 3 mM 4-phenylbutyric acid (PBA; an HDAC inhibitor, Sigma-Aldrich) for 72 h, replacing the drug and medium every 24 h. A total of 83 primary BCa specimens were collected from patients who underwent radical cystectomy (RC) or transurethral resection of bladder tumor (TURBT; 66 males and 17 females; median age: 72 yr; range: 34–90 yr). Of the 83 patients, 73 underwent surgical resection after initial diagnosis, 7 received chemotherapy before surgery, and 3 are recurrent cases. Samples of nontumorous bladder tissue adjacent (<2 cm) to and distant (>2 cm) from the tumors were also collected. Six samples of normal urothelial tissue from renal cell carcinoma (RCC) patients who underwent nephrectomy were also collected. Informed consent was obtained from all patients before collection of the specimens, and this study was approved by the institutional review board. Total RNA was extracted using a *mir*Vana miRNA isolation kit (Life technologies, Carlsbad, CA, USA). Genomic DNA was extracted using the standard phenol-chloroform procedure.

### 2.2. Urine samples

Voided urine specimens were collected from 20 cancer-free individuals (Supplementary Table 2) and 86 BCa patients. In addition, postoperative voided urine samples were collected from 36 of the 86 patients 3–10 d after TURBT treatment. As an independent test set, preoperative urine samples were collected from 34 BCa patients, and postoperative samples were collected from 11 patients. The postoperative urine samples were collected from patients in whom tumors were successfully resected without leaving residual tumors. The urine (10 ml) was mixed with 5 ml of ThinPrep PreservCyt solution (Hologic, Bedford, MA, USA) and stored at 4 °C. Each sample was centrifuged at 3000 rpm for 10 min, and genomic DNA was extracted from the pelleted sediment using the standard phenol-chloroform procedure.

### 2.3. MicroRNA expression profiling

Expression of 664 miRNAs was analyzed using a TaqMan MicroRNA array v2.0 (Life Technologies). Briefly, 1 μg of total RNA was reverse-transcribed using a Megaplex Pools kit (Applied Biosystems, Foster City, CA, USA), after which miRNAs were amplified and detected using polymerase chain reaction (PCR) with specific primers and TaqMan probes. U48 snRNA (RNU48, Life Technologies) served as an endogenous control.

### 2.4. Quantitative real-time polymerase chain reaction of miRNA

Expression of selected miRNAs was analyzed using TaqMan microRNA assays. Briefly, 5 ng of total RNA were reverse-transcribed using specific stem-loop real-time primers, after which they were amplified and detected using PCR with specific primers and TaqMan probes. U6 snRNA (RNU6B, Life Technologies) served as an endogenous control.

### 2.5. Methylation analysis

Bisulfite conversion of genomic DNA, methylation-specific PCR (MSP), bisulfite sequencing, and bisulfite pyrosequencing were carried out as described previously [8]. Primer sequences and PCR product sizes are listed in Supplementary Table 3. Primer locations for methylation analysis are shown in Supplementary Figure 1.

### 2.6. Transfection of microRNA precursor molecules

BCa cells ($1 \times 10^6$ cells) were transfected with 100 pmol of Pre-miR miRNA Precursor Molecules (Life Technologies) or Pre-miR miRNA Molecules Negative Control #1 using a Cell Line Nucleofector kit R (Lonza, Basel, Switzerland) with a Nucleofector I electroporation device (Lonza) according to the manufacturer's instructions. The viability of the miRNA precursor transfectants was analyzed using water-soluble tetrazolium salt (WST) assays [8]. Cell invasion was assessed using Matrigel invasion assays [8].

### 2.7. Gene expression microarray analysis

One-color microarray-based gene expression analysis was carried out according to the manufacturer's instructions (Agilent Technologies, Santa Clara, CA, USA). Briefly, 100 ng of total RNA were amplified and labeled using a Low-input Quick AmpLabeling Kit One-color (Agilent Technologies), after which the synthesized cRNA was hybridized to a SurePrint G3 Human GE microarray (G4851F; Agilent Technologies). The microarray data were then analyzed using GeneSpring GX version 11 (Agilent Technologies). The Gene Expression Omnibus accession number for the miRNA microarray data is GSE41760.

### 2.8. Statistical analysis

All data were analyzed using GraphPad Prism 4.0 statistical software (GraphPad Software, La Jolla, CA, USA). Quantitative variables were analyzed using a Student $t$ test and one-way analysis of variance (ANOVA) with a post hoc Tukey test. Fisher exact test was used for analysis of categorical data. The Pearson correlation coefficient was used to evaluate correlations between continuous data. Receiver operating characteristic (ROC) curves for the diagnosis of BCa were constructed on the basis of the methylation levels, followed by calculation of the area under the curve (AUC). The best cut-off value for each miRNA gene was defined as the point on the ROC curve closest to the upper left corner. A diagnostic scoring system using urinary DNA methylation was constructed by analyzing the training set using the following three-step algorithm: (1) The methylation status of miRNA genes was assessed using the respective cut-off values; (2) the number of methylation-positive genes was determined, which we termed the *miR-methylation score* (M-score); and (3) the samples were classified into five groups based on the M-score. The value of $p < 0.05$ (two-sided) was regarded as significant.

## 3. Results

### 3.1. Identification of epigenetically silenced microRNA genes in bladder cancer

To identify epigenetically silenced miRNAs in BCa, we performed TaqMan array analysis using two BCa cell lines (T24 and UM-UC-3) treated with 1 μM 5-aza-dC plus 3 mM PBA. Of the 664 miRNAs examined, the drug treatment induced upregulation (more than five-fold) of 208 miRNAs in T24 cells and 200 miRNAs in UM-UC-3 cells. Of those, 146 miRNAs were upregulated in both cell lines (Supplementary Fig. 2 and 3; Supplementary Table 4). We selected 23 miRNA genes that harbored CGIs in the proximal upstream (<5 kb) of their coding regions (Supplementary Table 5), and subsequent MSP analysis revealed that the CGIs of 12 were hypermethylated in multiple BCa cell lines (Fig. 1A). These miRNAs were also induced by a low dose (0.1 μM) of 5-aza-dC plus PBA, making it unlikely that the observed induction was a secondary effect of DNA damage (Supplementary Fig. 4).

We next used bisulfite pyrosequencing to quantitatively analyze the methylation of the 12 miRNA genes showing CGI methylation in a series of BCa tissues ($n = 26$), a sample of normal urothelium tissue, and a normal urothelial cell line (SV-HUC-1). We found that four miRNA genes (miR-137, miR124-2, miR-124-3, and miR-9-3) were frequently methylated in primary tumors, though their methylation levels were limited in normal urothelium (Fig. 1B; Supplementary Fig. 5 and 6). In addition, we observed a marked

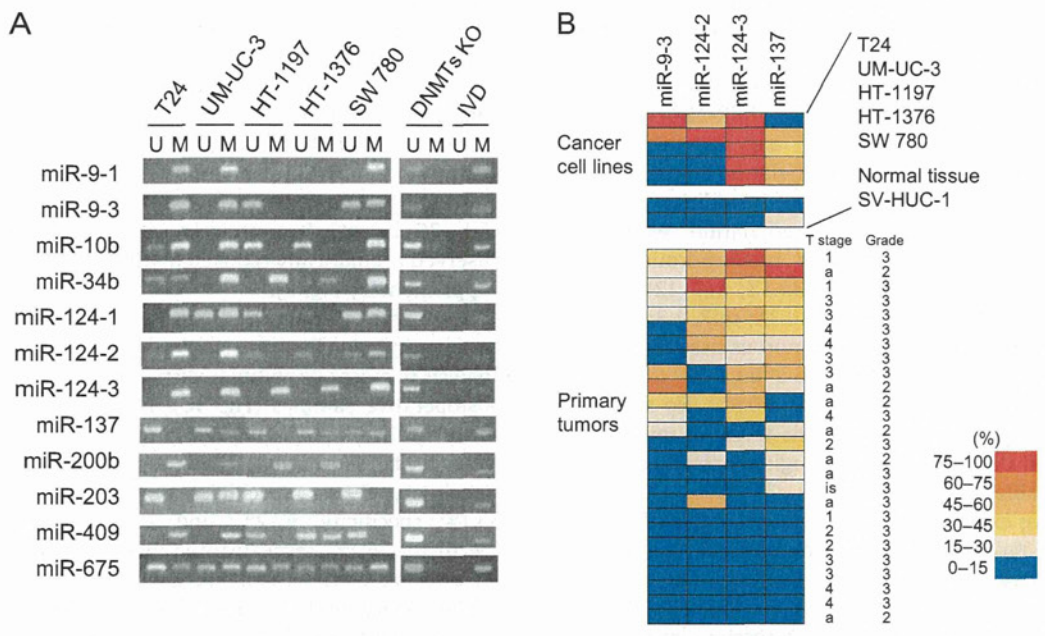


**Fig. 1 – Methylation analysis of microRNA (miRNA) genes in bladder cancer (BCa). (A) Methylation-specific polymerase chain reaction (PCR) analysis of the CpG islands of 12 miRNA genes in the indicated cell lines. In vitro methylated DNA and DNA methyltransferase knockout cells served as positive and negative controls, respectively. Bands in the "M" lanes are PCR products obtained with methylation-specific primers; those in the "U" lanes are products obtained with unmethylated-specific primers. (B) Summarized results for the bisulfite pyrosequencing of miRNA genes in BCa cell lines, a sample of normal urothelial tissue, a normal urothelial cell line SV-HUC-1, and a set of primary BCa tissues ($n = 26$). Tumor stages and grades are indicated on the right.**
**DNMTs KO = DNA methyltransferase knockout cells; IVD = in vitro methylated DNA.**

**Table 1 – Correlation between microRNA gene methylation and the clinicopathologic features of bladder cancer**

| | (*n* = 83) | miR-137 met (%) | | | miR-124-2 met (%) | | | miR-124-3 met (%) | | | miR-9-3 met (%) | | |
|---|---|---|---|---|---|---|---|---|---|---|---|---|---|
| | | Mean | SD | *p** | Mean | SD | *p** | Mean | SD | *p** | Mean | SD | *p** |
| Age, yr: | | | | | | | | | | | | | |
| Median (range) | 72 (34–90) | – | – | 0.394 | – | – | 0.277 | – | – | 0.147 | – | – | 0.065 |
| Gender: | | | | | | | | | | | | | |
| Male | 66 | 26.7 | 19.9 | – | 25.1 | 23.9 | – | 32.0 | 24.4 | – | 19.8 | 17.4 | – |
| Female | 17 | 34.6 | 22.1 | 0.160 | 22.2 | 11.1 | 0.630 | 31.8 | 20.6 | 0.974 | 17.3 | 13.0 | 0.591 |
| T stage: | | | | | | | | | | | | | |
| Ta | 35 | 31.3 | 23.4 | – | 25.1 | 22.1 | – | 29.7 | 25.2 | – | 21.0 | 18.5 | – |
| Tis | 4 | 23.5 | 19.7 | – | 24.6 | 28.8 | – | 22.5 | 15.4 | – | 12.7 | 4.4 | – |
| T1 | 8 | 33.4 | 19.2 | – | 33.9 | 29.9 | – | 42.6 | 25.2 | – | 24.9 | 16.2 | – |
| ≥T2 | 36 | 24.9 | 17.8 | 0.486 | 21.8 | 19.3 | 0.575 | 32.7 | 22.1 | 0.458 | 17.0 | 15.3 | 0.463 |
| Grade: | | | | | | | | | | | | | |
| 1 | 1 | 15.3 | – | – | 1.9 | – | – | 5.8 | – | – | 11.2 | – | – |
| 2 | 27 | 29.3 | 23.4 | – | 21.3 | 18.9 | – | 28.6 | 24.6 | – | 21.3 | 16.6 | – |
| 3 | 55 | 28.1 | 19.3 | 0.795 | 26.5 | 23.2 | 0.360 | 34.1 | 22.9 | 0.331 | 18.4 | 16.8 | 0.676 |
| LN metastasis: | | | | | | | | | | | | | |
| N0 | 73 | 28.6 | 21.0 | – | 24.9 | 22.4 | – | 32.4 | 24.0 | – | 20.1 | 17.3 | – |
| N1–N3 | 10 | 26.7 | 17.8 | 0.782 | 21.8 | 18.2 | 0.685 | 28.3 | 20.5 | 0.605 | 13.3 | 7.3 | 0.231 |

SD = standard deviation; LN = lymph node; ANOVA = analysis of variance.
* Pearson correlation coefficient, student *t* test, or ANOVA.

reduction in the methylation levels in BCa cells treated with 5-aza-dC plus PBA, which is consistent with the upregulation of miRNAs (Supplementary Fig. 7).

### 3.2. *Methylation of microRNA genes in primary bladder cancer*

We next examined the methylation levels of miR-137, miR-124-2, miR-124-3, and miR-9-3 in a larger set of primary tumors ($n = 83$), along with adjacent and distant nontumorous bladder tissues from the same patients (Table 1). Elevated levels of miRNA gene methylation (>15.0%) were frequently detected in primary BCa tissues (miR-137: 57 of 83, 68.7%; miR-124-2: 42 of 83, 50.6%; miR-124-3: 54 of 83, 65.1%; miR-9-3: 38 of 83, 45.8%), and the tumor tissues exhibited significantly higher methylation levels than their nontumorous counterparts (Fig. 2A). In addition, we found that levels of miRNA gene methylation were more frequently elevated in adjacent nontumorous bladder tissues (AN; miR-137: 26 of 74, 35.1%; miR-124-2: 19 of 74, 25.7%; miR-124-3: 15 of 74, 20.3%; miR-9-3: 12 of 74, 16.2%) than in more distant nontumorous tissues (DN; miR-137: 18 of 83, 21.7%; miR-124-2: 6 of 83, 7.2%; miR-124-3: 11 of 83, 13.3%; miR-9-3: 9 of 83, 10.8%). No significant correlation was found between the levels of miRNA gene methylation and the clinicopathologic characteristics of the patients (Table 1).

When we examined the methylation status of miR-137 in selected tissue specimens in more detail, we observed dense methylation in tumor tissues but only scattered methylation in nontumorous tissues (Fig. 2B). We then compared the levels of miR-137 expression determined in TaqMan assays with the methylation levels obtained by bisulfite pyrosequencing in selected pairs of tumors and corresponding distant nontumorous tissues (Fig. 2C). We found that there was an inverse relationship between the expression of miR-137 and its methylation, which suggests that CGI methylation is associated with the downregulation of miR-137 in BCa tissues.

### 3.3. *Detection of microRNA gene methylation in urine samples*

To assess the usefulness of miRNA gene methylation, we collected voided urine specimens from 86 BCa patients (Table 2) and 20 cancer-free individuals. Upon performing bisulfite pyrosequencing, we observed elevated methylation of miR-137, miR-124-2, miR-124-3, and miR-9-3 in the urine samples from the cancer patients (Fig. 3A) but only limited methylation of the genes in cancer-free individuals (Fig. 3B). Moreover, the methylation levels in the urine samples correlated positively with those in the corresponding tumor tissues (Supplementary Fig. 8). Notably, when we then collected postoperative voided urine samples from 36 of the 86 patients after surgical resection of their tumors, we observed dramatically reduced methylation levels (Fig. 3A; Supplementary Fig. 9).

To further evaluate the clinical usefulness of the miRNA gene methylation in urine samples, we carried out ROC curve analysis to assess its ability to distinguish preoperative from postoperative samples (Fig. 3C). The most discriminating cut-offs for miR-137, miR-124-2, miR-124-3, and miR-9-3 were 5.2% (sensitivity, 77.9%; specificity, 77.8%), 5.2% (sensitivity, 69.8%; specificity, 88.9%), 12.0% (sensitivity, 65.1%; specificity, 97.2%), and 7.2% (sensitivity, 69.4%; specificity, 86.1%), respectively (Table 3). We next compared these results with those obtained with urine cytology. Based on the urinary cytology using Papanicolaou's classification of the 86 patients, 55 (64%) were diagnosed as class I or II, 15 (17%) were class III, and only 16 (19%) were class IV or V (strongly suggestive or conclusive of malignancy), suggesting that the sensitivity of urinary methylation for detection of BCa is significantly greater than that of conventional cytology (Supplementary Table 6).

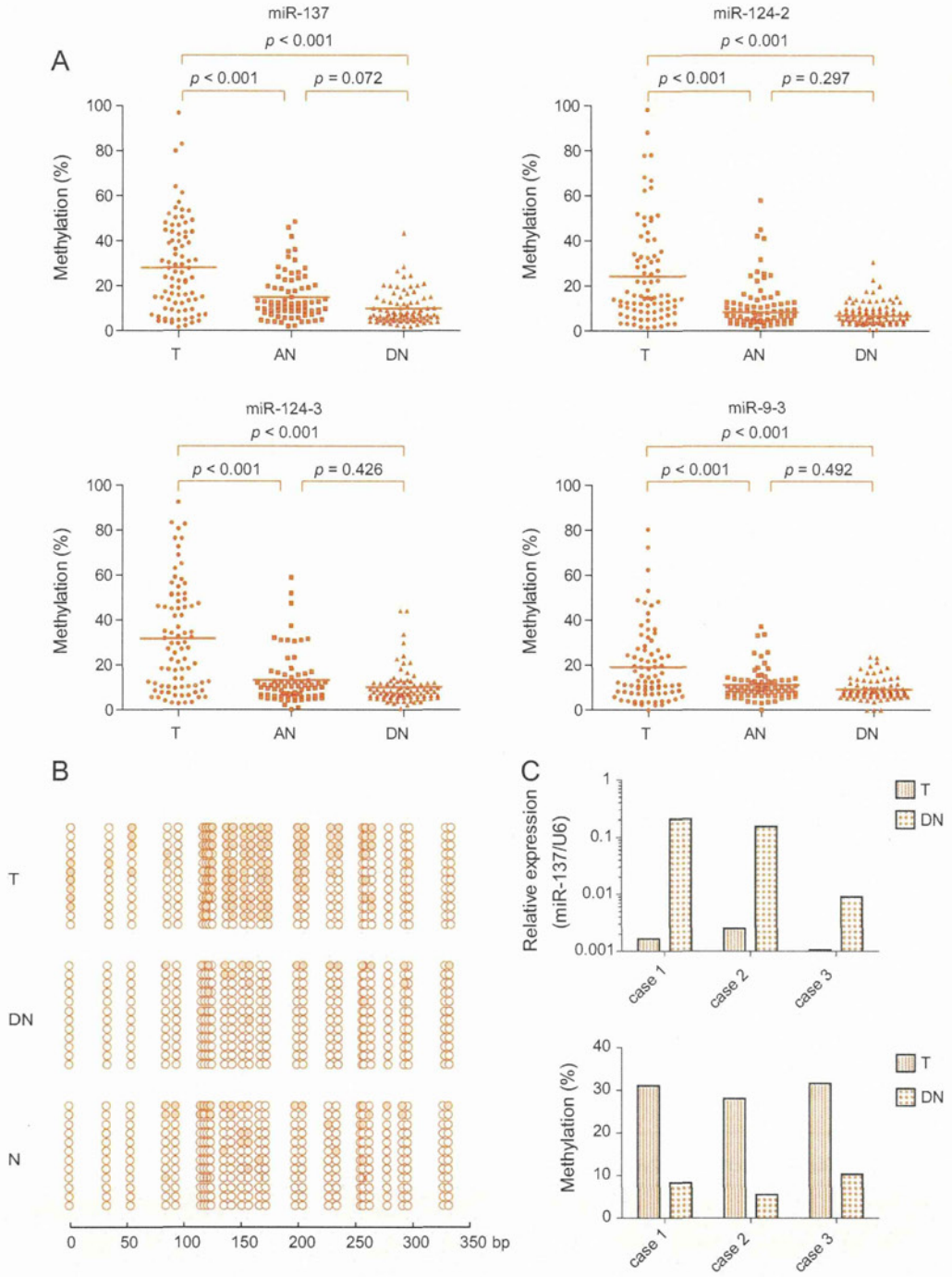


**Fig. 2 – Analysis of microRNA (miRNA) gene methylation in primary bladder cancer. (A) Summarized results of bisulfite pyrosequencing of the indicated miRNA genes in primary tumors (T; $n = 83$), nontumorous bladder tissues adjacent to the tumors (AN; $n = 74$), and nontumorous bladder tissues distant from the tumors (DN; $n = 83$). $p < 0.05$. (B) Bisulfite sequencing analysis of the miR-137 CpG island (CGI) in a pair of tumor (T) and distant nontumorous tissues (DN). (C) Inverse relationship between the expression and methylation of miR-137 in three pairs of tumor (T) and distant nontumorous tissues (DN). Expression was assessed in TaqMan assays (upper panel), and methylation was determined by bisulfite pyrosequencing (lower panel).**

To develop a more efficient diagnostic method for detecting BCa, we constructed a scoring system using the urinary methylation of the four methylated miRNA genes (Fig. 4). Using the cut-off value for each gene (Table 3), we classified the samples into five groups based on the M-score. A ROC curve was then constructed to evaluate the ability of the scoring system to distinguish preoperative from postoperative urine samples by plotting the sensitivity over 1-specificity at each point (Fig. 4B). We then validated the diagnostic system by analyzing an independent test set

**Table 2 – Clinicopathologic characteristics of the patients in the training and test sets**

| | Training set ($n$ = 86) | Test set ($n$ = 34) |
|---|---|---|
| Age, yr: | | |
| Median (range) | 73 (42–90) | 71 (58–93) |
| Gender, no.: | | |
| Male | 69 | 25 |
| Female | 17 | 9 |
| T stage, no.: | | |
| Ta | 34 | 16 |
| Tis | 7 | 5 |
| T1 | 12 | 8 |
| ≥T2 | 33 | 5 |
| Grade, no.: | | |
| 1 | 1 | 0 |
| 2 | 28 | 14 |
| 3 | 57 | 20 |
| Lymph node metastasis, no.: | | |
| N0 | 81 | 32 |
| N1–N3 | 5 | 2 |
| Treatment, no.: | | |
| TURBT | 64 | 30 |
| RC | 22 | 4 |

TURBT = transurethral resection of bladder tumor; RC = radical cystectomy.

(Table 2). AUCs in both sets were high (training set: 0.916; test set: 0.910), confirming the accuracy of our system for detecting BCa using urinary miRNA gene methylation (Fig. 4). We also found that our scoring system could effectively detect early-stage Ta and low-grade (grades 1 and 2) BCa (sensitivity: 0.679; specificity: 0.889; AUC = 0.862), which was undetectable using urinary cytology (Supplementary Fig. 10).

### 3.4. *Functional analysis of microRNAs*

To test whether any of the miRNAs could act as tumor suppressors, we transfected BCa cells with an miRNA precursor molecule or a negative control, and then carried out cell viability assays. The assays showed that ectopic expression of miR-137 or miR-124 suppressed BCa cell proliferation, whereas miR-9 exerted no significant suppressive effect on growth (Supplementary Fig. 11 and 12). We then carried out Matrigel invasion assays to test the effect of the miRNAs on cell invasion. Although we detected no effect of miR-137 and miR-124 on cell invasion, ectopic expression of miR-9 suppressed the invasiveness of BCa cells (Supplementary Fig. 13).

Finally, to further clarify the effect of miRNAs, we carried out a gene expression microarray analysis of SW780 cells transfected with a miR-137 precursor or a negative control. We found that 1326 probe sets (1016 unique genes) were downregulated (more than two-fold) by ectopic miR-137 expression, including the previously reported miR-137 target genes cyclin-dependent kinase 6 (*CDK6*), cell division cycle 42 (*CDC42*), and aurora kinase A (*AURKA*) [14,15]. Among the 1016 downregulated genes, the TargetScan program predicted that 144 genes are potential targets of miR-137 (Supplementary Table 7). Moreover, Gene Ontology analysis revealed that genes related to the cell cycle were significantly enriched among the affected genes (Supplementary Table 8). Our results strongly suggest that the miRNAs in question act as tumor suppressors in BCa.

## 4. Discussion

We identified four miRNA genes (miR-137, miR-124-2, miR-124-3, and miR-9-3) that were frequently methylated in both cultured and primary BCa cells. Earlier studies have shown that these miRNAs are tumor-suppressive or tumor-related and that they are epigenetically silenced in cancers of various origins. Hypermethylation of miR-137 was first discovered in oral cancer [16] and has since been noted in other malignancies, including cancers of the colon [14] and stomach [3]. Within cancer cells, miR-137 targets *CDK6*, *CDC42*, and *AURKA*, which is indicative of its tumor-suppressive properties [14–16], whereas in normal cells, miR-137 regulates neuronal differentiation through targeting enhancer of zeste homolog 2 (*EZH2*) and mindbomb E3 ubiquitin protein ligase 1 (*MIB1*) [17,18]. Methylation of miR-124 family genes (miR-124-1, miR-124-2, and miR-124-3) was identified in colorectal cancer [19] and was also

**Table 3 – Receiver operating characteristic analysis of microRNA gene methylation to detect bladder cancer**

| Gene name | Cut-off, % | Training set | | |
|---|---|---|---|---|
| | | AUC (95% CI) | Sensitivity (95% CI) | Specificity (95% CI) |
| miR-137 | 5.2 | 0.782 (0.701–0.862) | 77.91 (67.67–86.14) | 77.78 (60.85–89.88) |
| miR-124-2 | 5.2 | 0.769 (0.686–0.851) | 69.77 (58.92–79.21) | 88.89 (73.94–96.89) |
| miR-124-3 | 12.0 | 0.805 (0.730–0.880) | 65.12 (54.08–75.08) | 97.22 (85.47–99.93) |
| miR-9-3 | 7.2 | 0.778 (0.697–0.860) | 69.41 (58.47–78.95) | 86.11 (70.50–95.33) |
| Gene name | Cut-off, % | Test set | | |
| | | AUC (95% CI) | Sensitivity (95% CI) | Specificity (95% CI) |
| miR-137 | 5.2 | 0.816 (0.693–0.938) | 79.41 (62.10–91.30) | 63.64 (30.79–89.07) |
| miR-124-2 | 5.2 | 0.866 (0.758–0.975) | 79.41 (62.10–91.30) | 90.91 (58.72–99.77) |
| miR-124-3 | 12.0 | 0.901 (0.807–0.995) | 58.82 (40.70–75.35) | 100.0 (71.51–100.0) |
| miR-9-3 | 7.2 | 0.797 (0.660–0.934) | 76.47 (58.83–89.25) | 72.73 (39.03–93.98) |

AUC = area under the curve; CI = confidence interval.

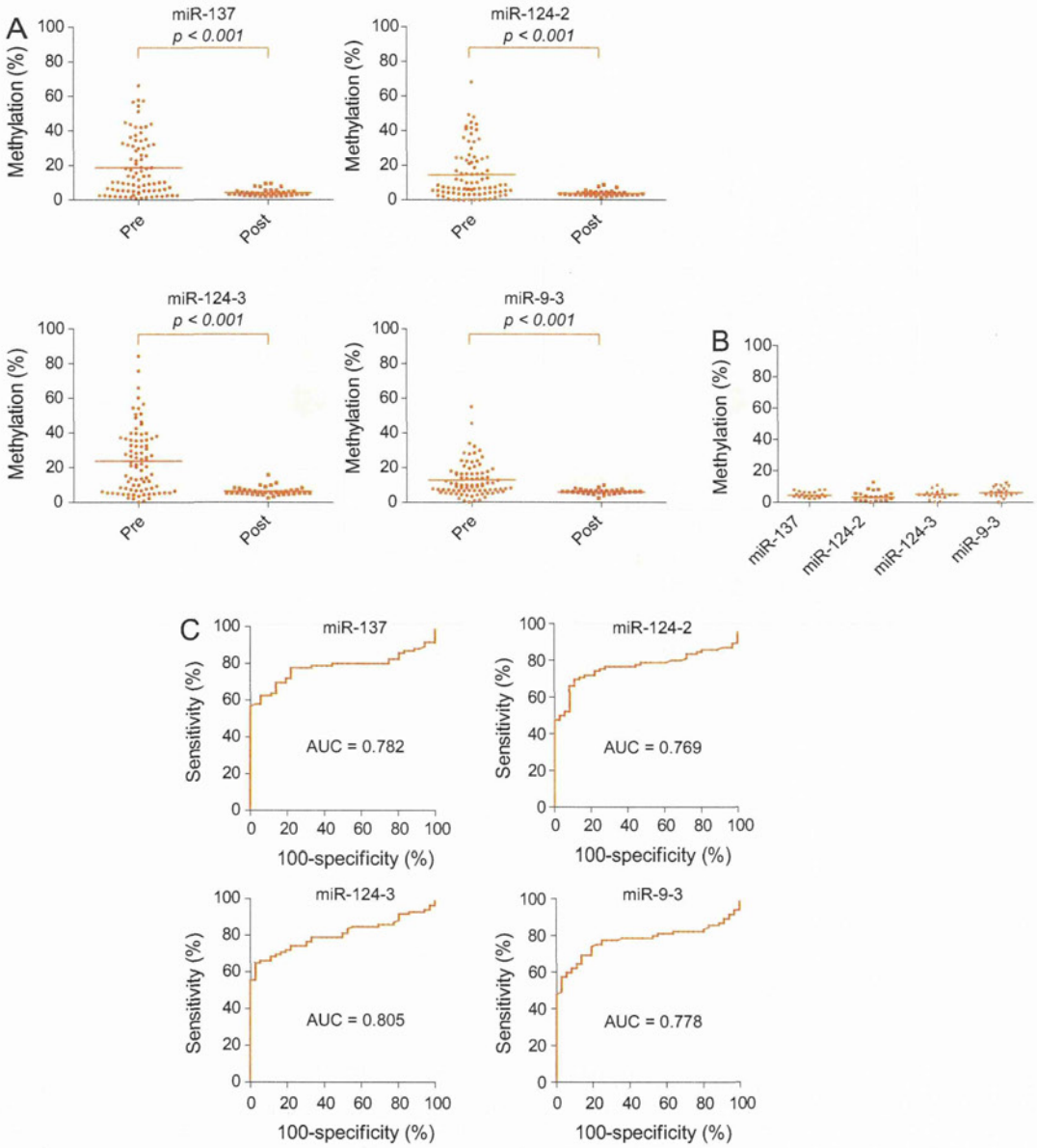


**Fig. 3 – Detection of microRNA (miRNA) gene methylation in urine specimens from bladder cancer (BCa) patients. (A) Summary of bisulfite pyrosequencing analysis of the indicated miRNA genes in voided urine samples collected from BCa patients before (Pre: $n = 86$) and after surgical treatment (Post: $n = 36$). $p < 0.001$. (B) Bisulfite pyrosequencing results for miR-137, miR-124-2, miR-124-3, and miR-9-3 in voided urine samples from cancer-free individuals ($n = 20$). (C) Receiver operating characteristics curve analysis of the ability of miRNA gene methylation to distinguish preoperative and postoperative urine samples.**
**AUC = area under the curve.**

found in gastric cancer [20], hematologic malignancies [21], and hepatocellular carcinoma [22]. In addition, screening for methylated miRNA genes in metastatic cancer cell lines also identified miR-9 family genes (miR-9-1, miR-9-2, and miR-9-3) [23].

Cumulative evidence suggests that miRNAs play important roles in the pathogenesis of BCa, and previous studies demonstrated their epigenetic silencing in the disease. For example, miR-34a, which is a direct target of p53 and a candidate tumor suppressor gene, is frequently methylated and silenced in many types of cancer, including BCa [24]. In addition, Wiklund et al. found that the silencing of miR-200 family genes and miR-205 is associated with DNA methylation in invasive BCa [12]. They also showed that reduced expression of miR-200c is associated with disease progression and poor outcome, suggesting that epigenetic silencing of miR-200 family genes could be a prognostic marker in BCa. Recently, Dudziec et al. carried out an miRNA microarray analysis after treating normal urothelium and urothelial cancer cell lines with 5-azacytidine. They identified 4 mirtrons and 16 miRNAs whose silencing was associated with DNA methylation [13]. Some of those

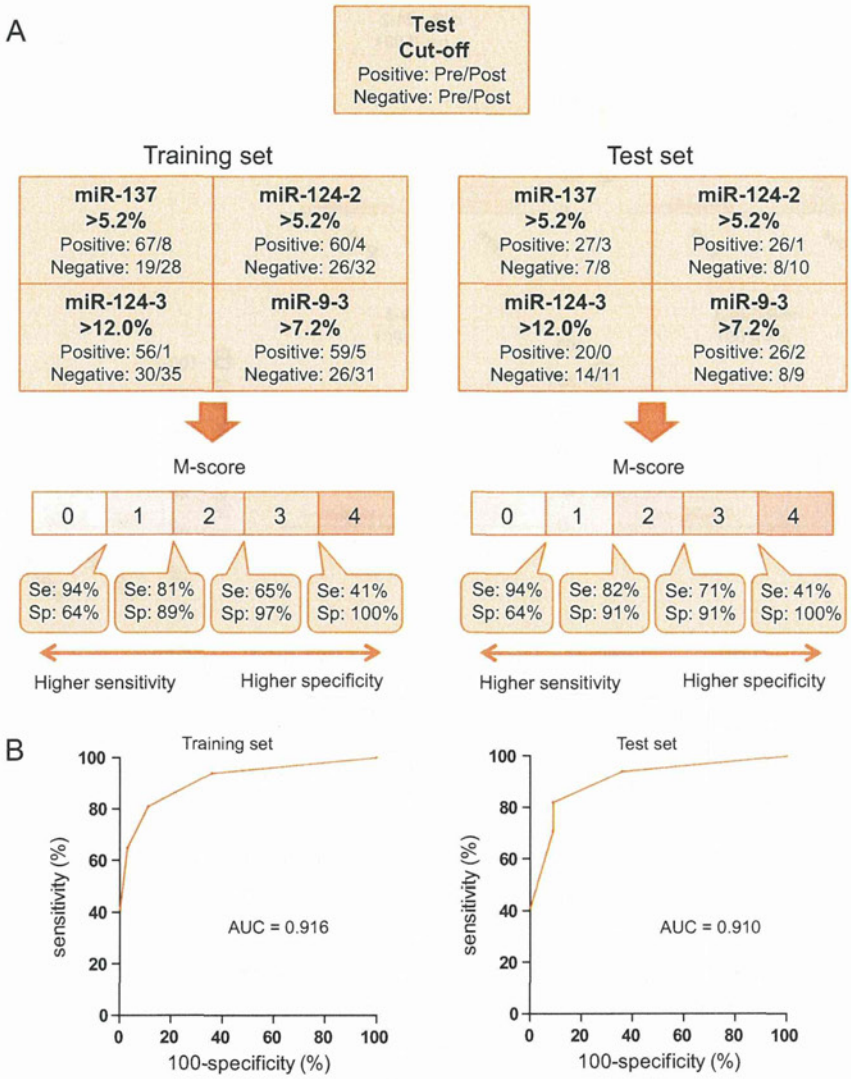


**Fig. 4 – Diagnostic system for detecting bladder cancer (BCa) using urinary microRNA (miRNA) gene methylation. (A) Workflow of a system established based on the ability to distinguish preoperative from postoperative urine. Results of the training set are shown on the left; those of test set are on the right. The methylation status of miRNA genes in preoperative (training set: *n* = 86; test set: *n* = 36) and postoperative urine (training set: *n* = 34; test set: *n* = 11) was determined using the cut-off values in the respective boxes. A miR-methylation score (M-score) was determined from the number of methylation-positive genes, and samples were classified into five groups based on the M-score. The sensitivity (Se) and specificity (Sp) at each point are indicated below. (B) Receiver operating characteristic curve analysis of the training and test sets. Areas under the curve are shown in the graph. M-score = miR-methylation score; AUC = area under the curve.**

mirtrons and miRNAs, including miR-9 family genes, more frequently exhibited CpG shore methylation than CGI methylation, suggesting that methylation in both the CpG shore and CGI is related to epigenetic silencing of miRNA in BCa. Interestingly, miR-9-1 and -9-2 were associated with both CGI and CpG shore methylation, whereas miR-9-3 showed only CGI methylation [13]. Consistent with those findings, we observed that among the miR-9 family genes, miR-9-3 most frequently showed CGI methylation.

Methylation of several miRNA genes is strongly related to the clinical characteristics of cancer, suggesting its potential usefulness as a biomarker. For instance, methylation of miR-9-1 and -9-3 is reportedly associated with metastatic recurrence of RCC, which is indicative of the possible role of miR-9 in cancer metastasis [25]. Despite this report, however, we did not find a significant difference in the levels of miR-9-3 methylation between noninvasive and invasive BCa tissues. Further study to clarify the functions of these miRNAs in BCa will be needed.

Recent studies have shown that miRNA levels in urine could serve as a molecular marker for detection of BCa. For instance, expression of miR-96 and miR-183 is reportedly upregulated in urothelial cancer, and their detection in urine strongly distinguished cancer patients from cancer-free patients [26]. Miah et al. also showed that evaluation of a panel of 10 miRNAs in urine is a highly sensitive method of detecting BCa [27]. DNA methylation is another potential molecular marker detectable in urine specimens. Several